Microstructural analyses of the addition of PP fibres on the fracture properties of high-strength self-compacting concrete by X-ray computed tomography

José D. Ríos[a], Jesús Mínguez[b], Antonio Martínez-De La Concha[a], Miguel Ángel Vicente[b] and Héctor Cifuentes[a*]

[a]ETS de Ingeniería. Universidad de Sevilla, Spain
[b]Department of Civil Engineering. Universidad de Burgos, Spain

*Corresponding author: bulte@us.es (Héctor Cifuentes)

Abstract

This paper analyses the influence of the presence of polypropylene fibres in the microstructure of a high-strength self-compacting concrete by X-ray computed tomography and its consequences on the mechanical and fracture properties. The addition of PP fibres alters the pore structure of the concrete matrix, and this affects the macroscopic response (i.e., mechanical and fracture behaviour). A microstructural analysis of an unreinforced concrete, used as reference mix, and two polypropylene fibre-reinforced mixes with two fibre length (6 and 24 mm) were experimentally carried out. Complementary, a comprehensive experimental study of the mechanical and fracture properties of each concrete were performed. Finally, it was established a correlation between the microscopic response (pore morphology and pore distribution) and the macroscopic behaviour of high-strength self-compacting concrete.

Keywords: high-strength concrete, polypropylene, fracture mechanic, X-ray computed tomography, microstructure.

1. Introduction

Self-compacting concrete (SCC) is regarded as one of the most used construction material worldwide [1,2] mainly due to the favourable properties in fresh (e.g. workability, pumpability, finishability) and hardened state (e.g. strength, density, permeability, durability) [3]. This concrete must be as fluid as possible with a stable mix to avoid segregation of solids. The fluidity is achieved commonly with the addition of super-plasticiser and/or viscosity modifying admixtures, and the stability of mix is obtained primarily through proper selection of powders (i.e., cement and cement replacement) [4]. Additionally, these characteristics conduct to a higher packing density (i.e., a reduction of porosity) which combined with the benefits of fibre addition derive to enhanced mechanical and fracture properties in comparison with vibrated concretes [2,3,5,6].

In self-compacting concrete with high compressive strength is very generalised the use of several industrial waste as cement replacement (e.g. fly ash, steel slag, rice husk) [7–11] and / or aggregate substitute (e.g., air-cooled blast furnace slag, masonry waste) [2,12,13] as

reflected by the high number of studies related to this issue. This behaviour conducts principally to two environmental benefits, the reduction of CO_2 emissions by the cement replacement, and complementary, the reuse of waste from several industries. Likewise, polypropylene fibres are also commonly added into the high-strength concretes [1,2,14–17]. The polypropylene fibres reduce the shrinkage effects [18] and enhance fire resistance [19]. Both the substitution of powder or aggregates as well as the fibre addition in the matrix alter the microstructure of concrete and the pore morphology [1,20,21]. Thus, the characteristics of fibres or constituents added have a significant influence in the microstructure and consequently, in the macroscopic response (i.e., mechanical and fracture properties).

The mechanical behaviour of concrete and especially its fracture behaviour, is strongly dependent on the porosity and pore distribution in the material [1,22–25]. There are three types of pores in cementitious matrix depending on the origin generation and their sizes. Gel pores, with characteristic dimensions between 0.5-10 nm; capillary pores, corresponding to the water-filled space ranging from 5 to 5,000 nm and macropores from entrained and entrapped air above 5,000 nm [20,23]. Gel pores have not a significant influence on the strength of material [23]. Nevertheless, capillary pores and macropores (i.e., those due to entrained or entrapped air) affect the strength and stiffness of concrete. There are a large number of researches which have studied the effect of pore structure on fibre-reinforced SCC (i.e., size, distribution, amount) by mercury intrusion porosimetry (MIP) technique [14–16,26]. However, this technique does not allow to capture data of larger pores (i.e., above 40 μm approximately) and the size of samples analysed is too small as being representative of real structural elements. X-ray computed tomography (CT) technique has being increasingly used on cementitious materials [27–31]. This technique allows to determine the geometry of pores (i.e., shape, size, sphericity, volume, etc.) and additionally, to analyse greater samples more representative of the structural elements in a three-dimensional scale.

The appearance of X-ray CT scanning to analyse the microstructure of cementitious materials is relatively recent. Numerous researches have used X-ray CT scan to determine the orientation and distribution of steel fibres on fibre-reinforced primarily concretes [24,29,31,32] since the significant difference of density between steel and concrete make this the ideal technique for this purpose. Nevertheless, there are scarce studies which have used X-ray CT technique in concrete reinforced with polymeric or plastic fibres because the small size of certain fibres makes more difficult their detection by X-ray CT scan. Pujadas et al. [33] analysed the orientation pattern of macro-plastic fibres by X-ray CT scan in which a predominantly perpendicular orientation to the flow of concrete was observed. The orientation of plastic fibres also was the aim of the study by Kaufmann et al. [34] by X-ray CT scan in a spray concrete. In this case, it was determined that the fibres were principally addressing to the perpendicular direction of spray.

Otherwise, some studies have been focused on the influence of pore structure of self-compacting concretes through MIP technique with different purposes. Mastali et al. [26] studied the effects of pozzolanic binders on the hardened-state properties of concrete. Saccani et al. [14] evaluated the effects in the interphase fibre-matrix of composites reinforced with

carbon fibres. However, the most common focus on interest is the thermal effects in the matrix. Missemer et al. [16] characterised the sensitivity of fibre-reinforced concrete to spalling and proposed a critical quantitative factor to determine a fire-resistant composition. Yermark et al. [35] presented a comprehensive study which correlated the mechanical properties with the thermal damage of concrete. Although there are a significant number of studies that have studied the mechanical [19,36–38] and fracture properties [39–42] of self-compacting concrete, scarce investigations have been focused on the porosity evolution inside concrete and the correlation with the macroscopic response (i.e. mechanical and fracture properties).

This work is focused on the effect that the addition of polypropylene fibres in the microstructure of high-strength self-compacting concrete (HSSCC) and its influence on the mechanical and fracture properties. For this, a plain concrete, used as reference concrete, and two PP fibre-reinforced concretes were experimentally assessed. The microstructural analysis of the matrix was performed by X-ray computed tomography technique. Finally, it was established a correlation among the microstructural results obtained by X-ray computed tomography and the mechanical and fracture behaviour of each concrete. The influence of the presence of PP fibres as well as the pore morphology in the fracture mechanisms have been comprehensively analysed.

This paper is organised as follows: a presentation of the materials manufactured, and a description of the sample preparation are shown in Section 2. A description of the experimental programme is exposed in Section 3. The results and discussion are presented in Section 4, and finally, the conclusions are found in Section 5.

2. Materials

2.1 Raw materials and mix designs

In this research, three concretes composed of the same constituents, except that instead of polypropylene fibres, have been manufactured. The mixes were designed following the method proposed by Karihaloo and Ghanbari [43], and Deeb and Karihaloo [44] for self-compacting ordinary and high-strength concretes. The nomenclature and fibre content of the mixes are presented in Table 1. The former mix, used as control concrete, is an unreinforced concrete and it is denoted as PC (plain concrete). The second and third of concretes mixes are reinforced with two types of PP fibres. The properties of PP fibres used are the same, except that of length, as can be seen in Table 1. The mix labelled as SFC (short-fibre concrete) contains PP fibres of 6 mm in length and the mix designated as LFC (long-fibre concrete) has fibres of 24 mm in length. The amount of PP fibres added to the mixes was the same in both cases (i.e., SFC and LFC) as well as the properties of PP fibres (i.e., thickness and toughness, see Table 1). The PP fibre length is the only difference so that the study is focused on the influence of fibre length in the microstructure of mixes.

Table 1 : Nomenclature of mixes, PP fibre content and properties.

	fibre type	fibre content (kg/m^3)	thickness (µm)	toughness (MPa)
PC[a]	no fibres	0	-	-
SFC[b]	6 mm in length	1.2	33	450
LFC[c]	24 mm in length	1.2	33	450

[a] plain concrete, [b] short-fibre concrete, [c] long-fibre concrete.

The mix proportions of constituents used are shown in Table 2. The concrete paste has a low water-to-binder ratio which infers a higher performance in terms of mechanical properties to the control concrete (i.e., PC). The binder is formed by type II Portland cement and densified silica fume of 0.1 µm particle size. Three types of aggregates are used (Table 2), one designated as fine silica sand, with a maximum particle size of 1 mm, coarse silica sand with a maximum particle size of 10 mm and a limestone sand with 2 mm of maximum size. The grading distribution of the aggregates are shown in Fig. 1.a. A third-generation polycarboxylate-based superplasticiser is used as water reducer. Slump flow tests of each mix, according to EFNARC recommendations [45], were conducted in order to ensure the flowability of concrete paste without segregation (Fig. 1.b).

Table 2 : Mix compositions of plain concrete (kg/m^3)

w/b[a]	cement[b]	silica fume	fine silica sand	coarse silica sand	limestone sand	water	superplasticiser
0.17	657	99	867	1301	139	131	23

[a] w/b water-to-binder ratio, [b] Portland cement (CEM II B-L 32.5 N).

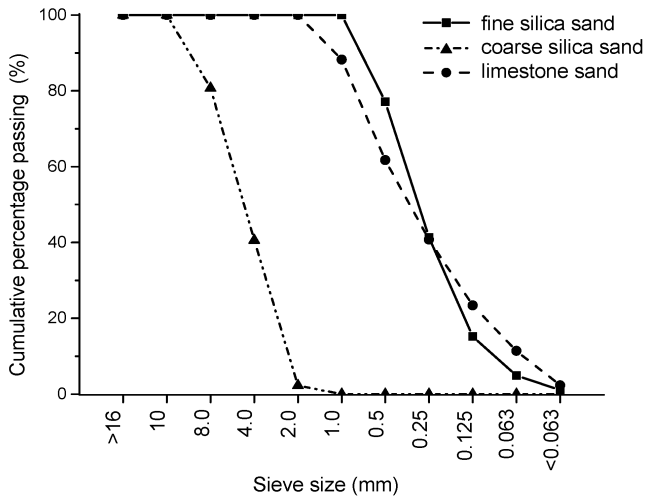

(a)

(b)

Fig. 1: Grading distribution of aggregates (a) and slump flow test of LFC mix (b).

2.2 Sample preparation

The specimen production was always carried out following the same mixing procedure in order to ensure minimising the experimental scattering. A laboratory horizontal rotary mixer was used for the manufacturing of mixes. First the constituent with coarser particle size (i.e., coarse silica sand) is poured in the mixer during the mixing process, next the finer particle size constituent (i.e., silica fume) is added and so, alternatively and subsequently, with the rest of dry constituents (i.e., limestone aggregate, cement and fine silica sand respectively). All dry constituents are mixing for 5 min to ensure a uniform mix. Then, a mix of the water and superplasticiser is poured, and it is mixed for 10 min. When a self-compacting paste is reached the PP fibres are added (for SFC and LFC mixes) and then mixed for 5 min more until fibres are homogeneously dispersed in the concrete paste (Fig. 1.b). The specimens were demoulded after casting for one day and stored in water at ambient temperature for 27 days more. After curing time, the specimens were dried at ambient temperature for 1 day.

3 Methods

In this section, the X-ray CT scanning and the mechanical and fracture tests performed are described.

3.1. Microstructural analysis by X-ray CT scan

X-ray computed tomography scans were carried out for each mix in order to obtain the effect of two PP fibre length (i.e., length of 6 mm and 24 mm) on the microstructure of self-compacting high-strength concrete. For this, three samples of each mix (PC, SFC and LFC) have been scanned in order to minimise the scattering derived from the intrinsic heterogeneity of the material. The samples scanned by X-ray CT had a dimension of 25×25×100 mm^3 and were sawn from beam specimens of 100×100×440 mm^3 casted. A schematic view of the specimen and the samples extracted is shown in Fig. 2. The samples were sawn from the core of the specimen and the same part for each mix to avoid border effects that might alter the microstructure of matrix, and consequently, the X-ray CT results obtained.

The CT scan used was a GE Phoenix v|tome|x device (General Electric, Boston, MA, USA), belonging to the 'Centro Nacional de Investigación sobre la Evolución Humana (CENIEH)', in Burgos, Spain. It is equipped with a tube of 300 kV/500 W. This facility emits a cone ray, which is received by an array of detectors. Thereby, the scanning process is fast, and highly accurate scans are produced of equal resolution in the X, Y, and Z axes.

The CT scan provides 16 bits pictures of 2,048×2,048 pixels. From each specimen we obtained 5,000 section images with a pixel size of 0.02. Also, the separation of each section slice was 0.02 mm.

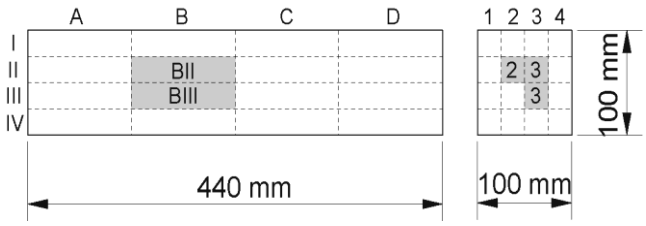

Fig. 2: Scheme of X-ray samples sawn.

Multiple 2D radiographs of each sample scanned were taken by X-ray CT with a scanning resolution of 1,024×1,024 pixels. The commercial software AVIZO was used for the 3D reconstruction of samples scanned (Fig. 3.a, b and c) and the subsequent microstructural analysis of pore properties (i.e., pore equivalent diameter, sphericity, pore surface and shape coefficient). The beam hardening and ring effects [28] were reduced by post-process tools from the analysis software. The equivalent diameter corresponds to the diameter of a sphere with the same volume of the pore, and it is defined as:

$$d_{eq} = \sqrt[3]{6V_{pore} / \pi} \quad (1)$$

Whereby V_{pore} is the volume of a pore. The sphericity of a pore represents how closely the shape of a pore approaches that of a perfect sphere and is defines as:

$$\varphi = \frac{\pi^{1/3}\left(6V_{pore}\right)^{2/3}}{A_{pore}} \quad (2)$$

whereby V_{pore} is the volume of a pore and A_{pore} is the surface area of a pore. The sphericity of a sphere is one and any pore which is not a sphere will have values below 1. The pore surface corresponds to the total area that the surface of the pore occupies. The shape coefficient is a dimensionless property that describes the shape of a pore independently of its size and it is defined as:

$$\alpha = \frac{A_{pore}{}^{3}}{36\pi V_{pore}{}^{2}} \quad (3)$$

For more detailed information about the X-ray CT analysis procedure, see the previous work by Rios et al. [32].

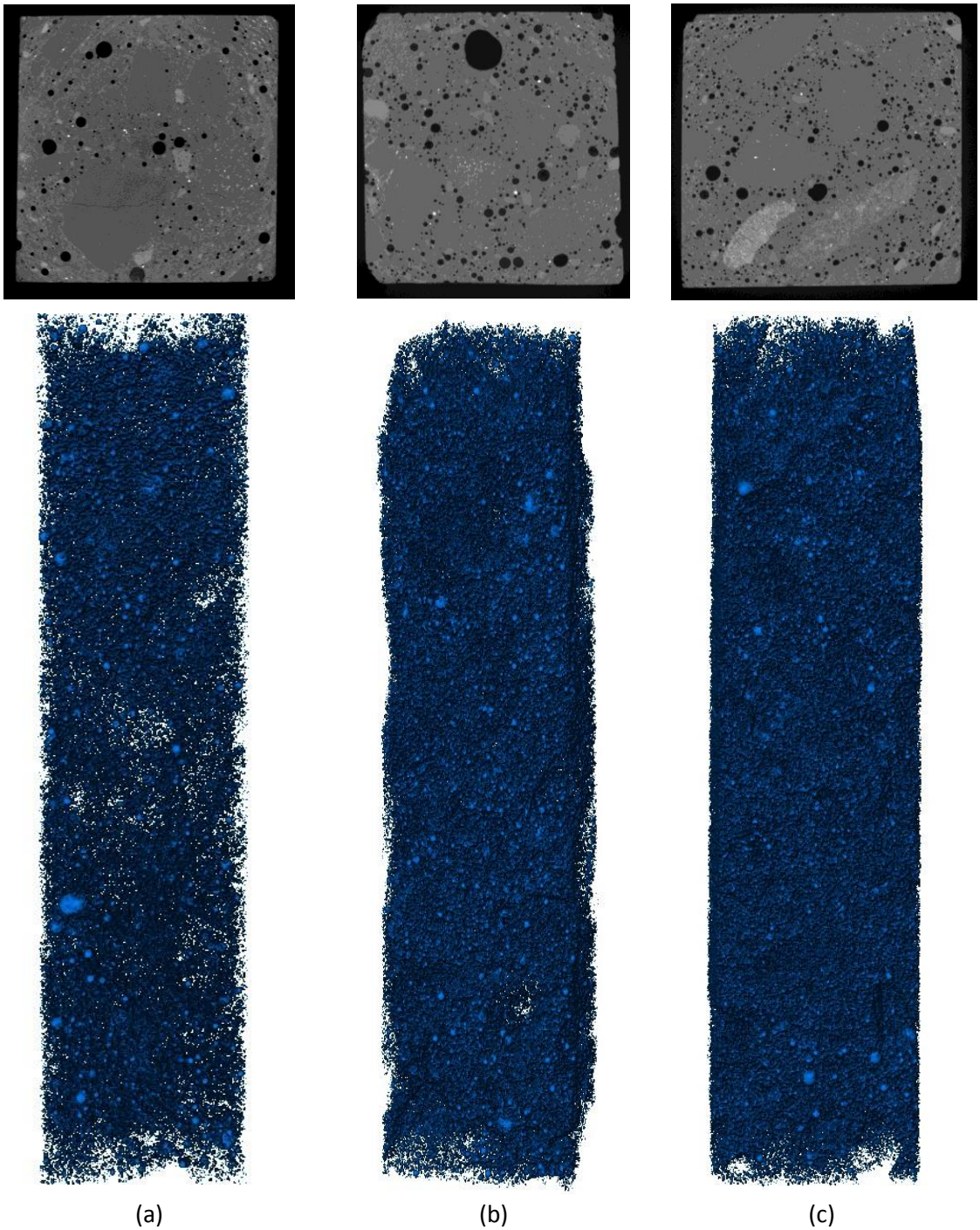

(a) (b) (c)

Fig. 3 : 3D reconstruction of each samples scanned by X-ray CT (a) PC, (b) SFC and (c) LFC mix.

3.2. Mechanical property tests

The compressive strength, f_c, of each mix (i.e. PC, SFC and LFC) were measured from the testing of cubic specimens of 100 mm of side. Four cube specimens of each mix were tested in accordance with the European standard EN-12390-3:2009 [46]. A servo-hydraulic machine of 3,000 kN as maximum load capacity was used with a loading rate of 0.5 MPa/s. The Young's modulus, E_c, was determined by cylindrical specimens of 100 mm diameter and 200 mm height according to the EN-12390-13:2014 [47]. Four specimens were tested of each mix (i.e., PC, SFC

and LFC) and the same servo-hydraulic machine used for compression was used. The procedure consists on the application of a gradual loading until a third of its failure load, and simultaneously, the relative strain is measured by two linear variable displacement transducer (LVDT) sensors of 25 mm in length.

3.3. Fracture property tests

Four specimens of each mix (i.e., PC, SFC and LFC) were conducts on three-point bending tests on notched prismatic specimens of 100×100×440 mm^3 (B×D×L) and notch depth, a, of 50 mm to determine the size-independent fracture energy, G_F, by the RILEM method [48] and considering the recommendations suggested by Guinea et al. [49–51]. The tests were conducted on a servo-hydraulic dynamic machine of ± 200 kN and the deflection at the midspan of the specimen was measured by an LVDT sensor of 25 mm. The sensor was mounted on a rigid frame fixed to the specimen. Additionally, the bilinear tension softening diagrams (Fig. 4) of each mix (i.e., PC, SFC and LFC) were determined by the use of an inverse analysis method based on the non-linear hinge model [52,53]. The method is based on the fictitious crack model which is commonly used for the analysis of cracked concrete structures using finite element models [53]. The bilinear softening diagram is defined by the tensile strength, f_t, the slope of the first linear branch, a_1, the slope of the second linear branch, a_2, and its intersection with the ordinate axis, b_1.

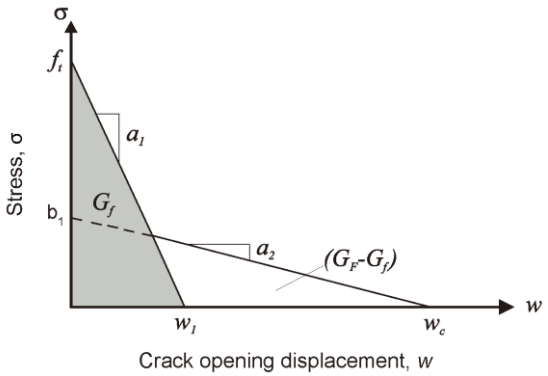

Fig. 4: Bilinear tension softening diagram.

The bilinear tension softening diagram is a proper way to analyse the effect of microstructure in concretes since it provides information about the micro-cracking and frictional dissipation processes responsible for the post-peak behaviour in concrete [39]. The initial fracture energy, G_f, corresponding to the area under the first linear branch (grey zone in Fig. 4), is depending on the microcracking process, while the second linear branch is a result of the frictional dissipation (e.g. aggregate interlock or fibre adherence) [39,54]. That information can be correlated with the X-ray CT results and establish a connection between microstructure and fracture behaviour.

On the other hand, it has been calculated the characteristic length, l_{ch}, which is a fracture parameter that provides information about the intrinsic brittleness of the cohesive material [55]. It is directly related to the fracture process zone (FPZ) due to a greater characteristic

length, higher FPZ [56]. Since all specimens tested had the same dimensions, there was no size effect, and an analysis of the ductility of mixes could be carried out. The characteristic length was calculated as according to Eq. 6:

$$l_{ch} = \frac{G_F E_c}{f_t^2} \quad (6)$$

4 Results and discussion

In this section are shown the results obtained by the X-ray computed tomography so that the effect of PP fibres on the microstructure of mixes can be related with the mechanical and fracture behaviour.

4.1 Microstructural analysis

The use of X-ray CT scan to analyse the microstructure of concrete allows the determination of a wide information about the pore properties (e.g., pore size, surface area, sphericity, etc.) with an accuracy of 40 μm in a large volume of material (Fig. 4). This leads to obtain more reliable results of microstructure in comparison with other techniques in which the volume of material analysed is remarkably more reduced (e.g., mercury intrusion porosimetry). Four prismatic samples of 100×25×25 mm^3 were analysed by X-ray CT scan for each mix (PC, SFC and LFC) and an average value of each pore property measured was obtained in order to reduce the scattering of results due to intrinsic heterogeneity of microstructure [57]. In this work, pores with less than 0.03 voxels (i.e., below 0.1 mm length approximately) are discarded because they are too small to be identified with enough definition [25].

From the X-ray CT results, the diagrams of the equivalent diameter of pores (abscissa axis) and its frequency (ordinate axis) are shown in Fig. 5 and 6 for each mix (PC, SFC and LFC). Pore equivalent diameter in a range between 0.10 and 0.60 mm is presented in Fig. 5 and a detailed diagram of the range of smaller pores, between 0.100-0.225 mm, is shown in Fig. 6 to be more clearly observed. The frequency of pores higher than 0.60 mm is significantly low so that it has not been shown in Fig. 5 since it does not provide relevant information.

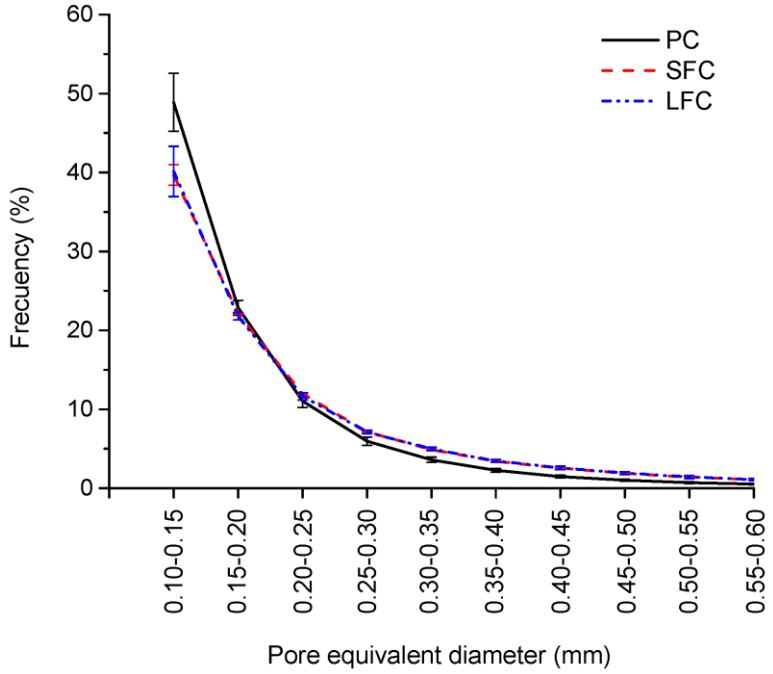

Fig. 5: Distribution of pore equivalent diameter of mixes.

From the results of Fig. 5, it is observed as the control concrete (i.e., PC) has a microstructure with a predominant concentration of pores in the smaller equivalent diameter, the 50% of pores are in the range of 0.10-0.15 mm (see Fig. 5). The presence of polypropylene fibres (SFC and LFC mixes) reduced the number of smaller pores (i.e., between 0.10 and 0.20 mm). The equivalent diameter between 0.10-0.15 mm was reduced 10% in comparison with the control concrete (i.e., PC), due to the air bubbles concentration inferred around fibres according to the results obtained by other authors [21,32]. This conducts to an increment of the equivalent diameter, due to pore fusion by concentrated air bubbles, in the range of pore size 0.25-0.60 mm (see Fig. 5). It is not observed significant differences in the microstructure of those mixes with PP fibres (SFC and LFC), as observed in the overlapping of their curves.

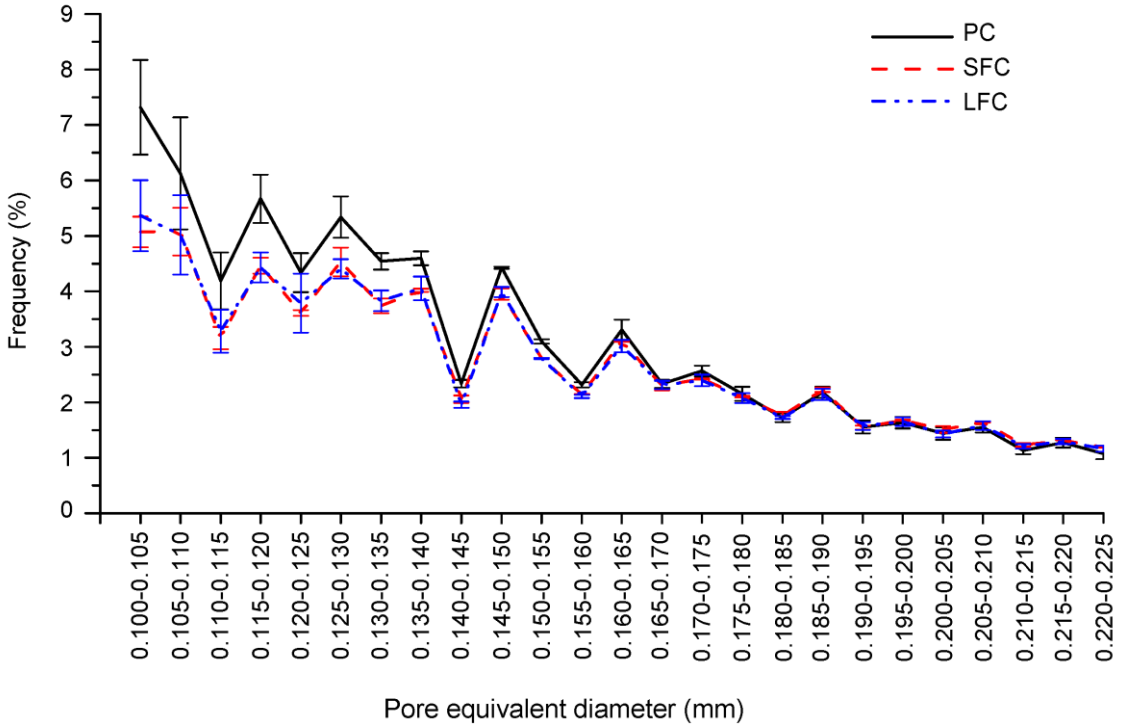

Fig. 6: Pore equivalent diameter of mixes with diameter below 0.225 mm.

Fig. 6 presents the information about those pores with equivalent diameter below 0.22 mm since it has been observed that the presence of PP fibres affects significantly to these pores and it was not able to observe changes, clearly, in the scale of Fig. 5. As observed, the control concrete (PC) has pores with smaller equivalent diameter than those reinforced with PP fibres (SFC and LFC) in the range between 0.100-0.175 mm. That difference is more remarkable for diameter size below 0.140 mm (see Fig. 6). This confirms that the addition of PP fibres increases the pore size by air bubbles concentration around fibres [21,32], as was seen in Fig. 5. The variation on the amount of pores with equivalent diameter between 0.175-0.225 mm is almost non-existent.

Table 3 : Pore density of mixes.

Mix	Pore density (pores/cm^3)				Total porosity (%)
	> 1 mm^3	1-0.5 mm^3	0.5-0.1 mm^3	<0.1 mm^3	
PC	2.0 ± 0.5	2.3 ± 0.6	27 ± 8	4423 ± 1309	2.6 ± 0.7
SFC	2.5 ± 0.5	4.2 ± 0.8	57 ± 5	6923 ± 608	5.4 ± 0.3
LFC	2.2 ± 0.6	3.1 ± 1.3	55 ± 24	10555 ± 444	7.0 ± 0.4

Table 3 presents pore density (in pores/cm^3) for pore volumes higher than 0.1 mm^3, in which the number of pores is low and, as a consequence, those pores could not be shown in Fig. 5 and 6. With regards to the control concrete (PC), it is the mix with a lower number of pores for any volume higher than 0.1 mm^3. This confirms that the plain concrete has a microstructure with pores of a smaller size than those with fibres [32]. In the PP fibre reinforced concretes (SFC and LFC), the mix with shorter PP fibres (SFC) presented significantly less amount of pores

below 0.1 mm^3 in comparison with that with longer PP fibres (LFC). The higher fibre-matrix interface led to a more significant pore concentration around fibres than in that case of short fibre concrete (SFC). Nevertheless, it was not observed a significant alteration of microstructure relative to those pore volumes higher than 0.1 mm^3 between SFC and LFC mixes. It can be confirmed that the PP fibre length studied (6 and 24 mm) has a significant influence only in those pores with volumes below 0.1 mm^3.

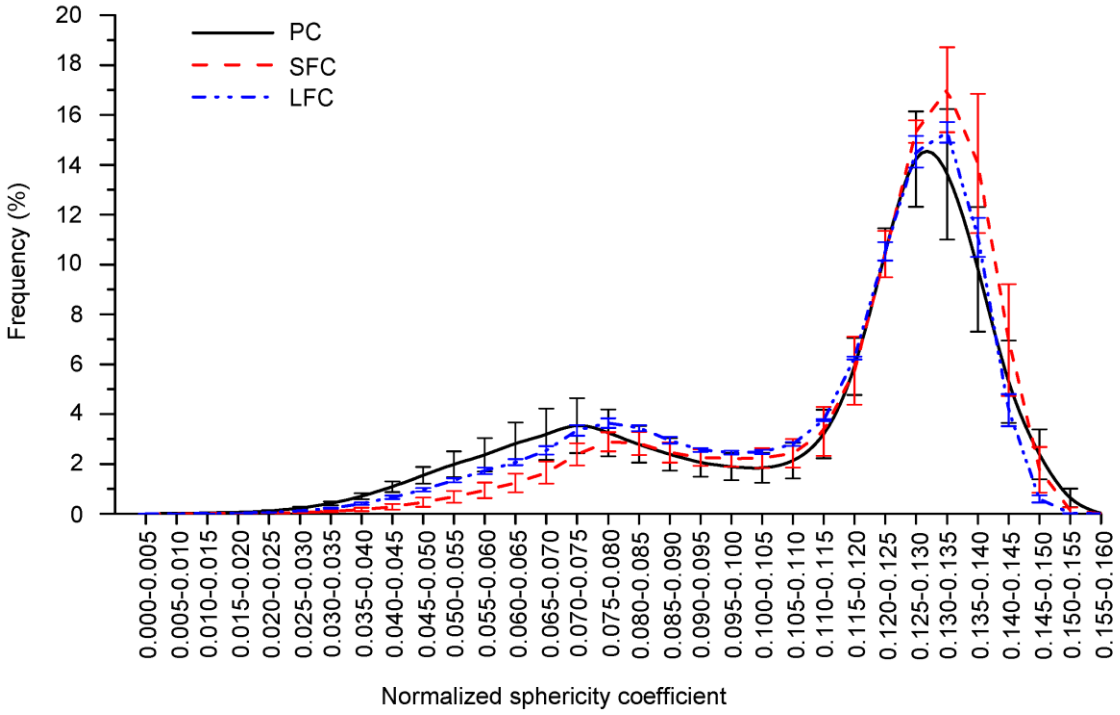

(a)

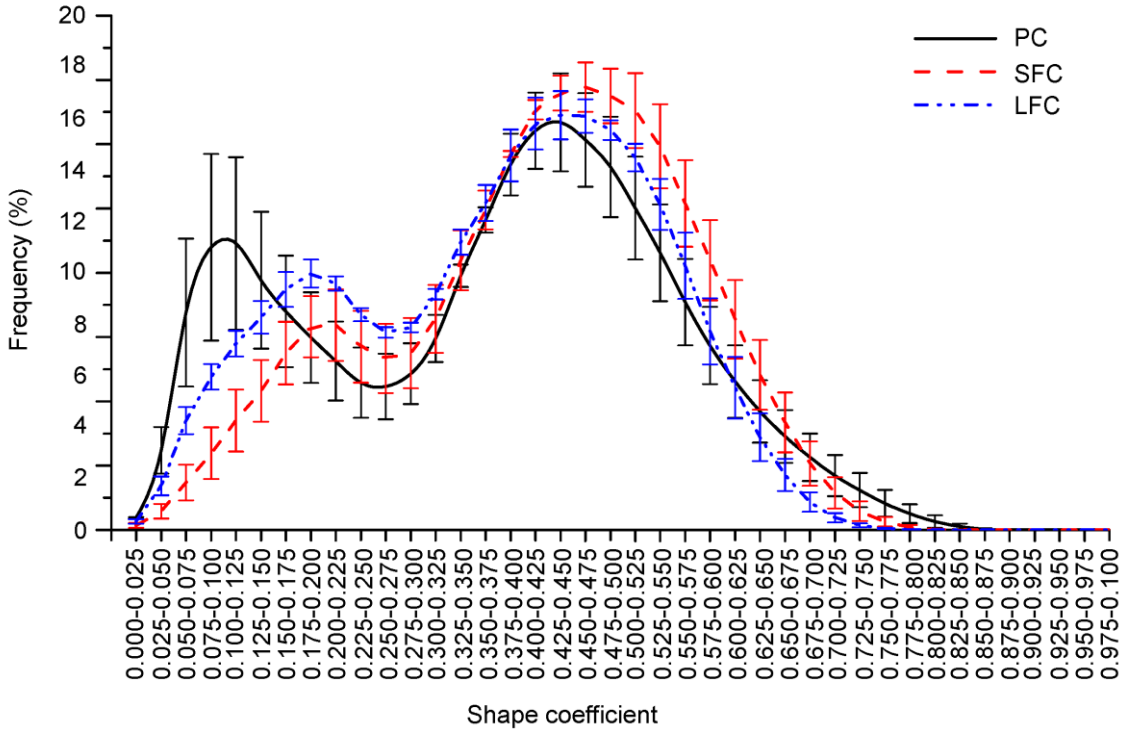

(b)

Fig. 7 : Sphericity (a) and shape coefficient (b) of pores for each mix.

Fig. 7 shows the values of the sphericity and shape coefficient of pores for each mix (PC, SFC and LFC). Both properties, the sphericity and shape coefficient, are an indication of the pore shape, which is related to each other as follows: $\varphi = \frac{1}{\alpha^{1/3}}$. For this reason, the discussion of the results is made jointly. The range of sphericity values (Fig. 7.a) varies between 0.000-0.160, which shows that the shape of pores is not very spherical for any mix, control (PC) or PP fibre-reinforced concrete (SFC and LFC). With regards to PP fibre reinforced mixes, the join of air bubbles generated beneath fibres leads to a higher sphericity (Fig. 7.a) and shape coefficient (Fig. 7.b). This was observed in the horizontal displacement (i.e., into higher spherical pore) of the peak points of Fig. 7.a and b for SFC and LFC mixes in comparison with PC mix. Additionally, there is a decrease of the shape coefficient in the range 0.150-0.175 and a complementary increase in the range 0.475-0.500 that confirms as pores are more spherical. This fact is more remarkable if the PP fibres are shorter (i.e., SFC) than longer (i.e. LFC) due to the decrease in the range of 0.150-0.175 of shape coefficient is significantly higher than LFC. By contrast, the increase in the range 0.475-0.500 of shape coefficient is higher than LFC mix.

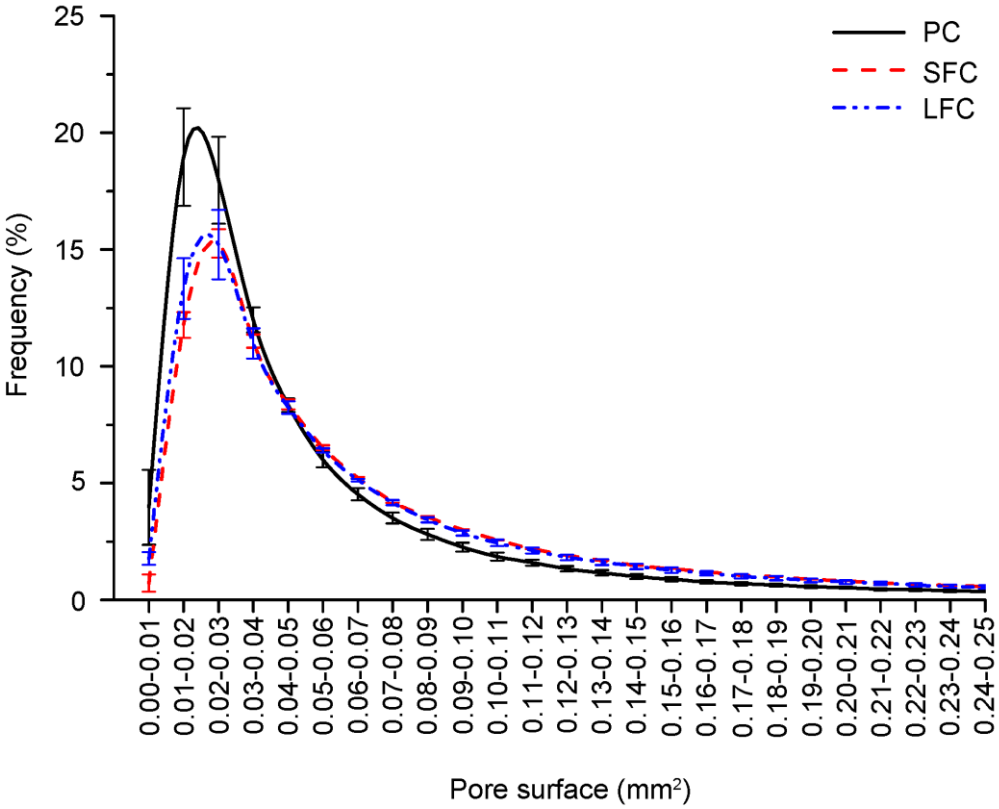

Fig. 8 : Pore surface of each mix

The pore surface results for each mix (PC, SFC and LFC) are shown in Fig. 8. From the control concrete (i.e., PC), there is a higher number of pores with surface area lower than those in PP fibre reinforced mixes (SFC and LFC). As shown, the 20% of pores are in the range of pore

surface between 0.01-0.04 whereas the PP fibre reinforced mixes (SFC and LFC) have a 16% in the same interval (see **Error! Reference source not found.**). The mesh of air bubbles generated around PP fibres leads to pores with higher volumes (as shown Table 3) and more spherical (Fig. 7**Error! Reference source not found.**.a and b) so that the surface area of pores must be higher, as shown in Fig. 8.

4.2 Mechanical properties

The average value of the compressive strength and Young's modulus, corresponding to the tests described in the previous section, and their standard deviation are shown in Table 4 for each SCC mix.

Table 4 : Average mechanical properties and standard deviation.

Mix	f_c (MPa)	E_c (GPa)
PC	80.0 (7.4)	38.9 (3.4)
SFC	77.2 (3.9)	40.9 (1.1)
LFC	75.2 (4.8)	43.2 (1.7)

From the results of compressive strength, it is observed as the addition of PP fibres conducted to a slight decrease of 3.5% for SFC and 6% for LFC. Other authors observed this fact in similar conditions [20,58]. This decrease was due to the inclusion of a material less resistant (i.e., polypropylene fibres) to the compressive stresses during the test and the alteration of microstructure by the presence of PP fibres, as presented in total porosity results (Table 3). The incidence of microstructure on the compressive strength of cement-based materials has been significantly studied by several researchers [22,23,25,59]. Many relationships that are establishing a connection between the compressive strength and pore structure of material have been obtained [22,59]. Thus, the decrease of compressive strength by the addition of PP fibres is due to the inclusion of a material less resistance (i.e., polypropylene fibres) and, additionally, to the increase of the total porosity, the pore size and amount of pores lower than 0.1 mm^3, due to the concentration of air bubbles around fibres reflected by the higher values of equivalent diameter (Fig. 5 and 6) and density (Table 3) respectively.

Regarding Young's modulus, the PP fibre reinforced mixes (SFC and LFC) slightly increased, 5.1% on SFC and 11% on LFC, following the results obtained by other authors [20,60,61]. As known, this property is primarily influenced by a higher number of pores with a size of nanometres, rather than a lower amount of pores with larger sizes [62]. From the results shown in Fig. 6, it is observed that the addition of PP fibres decreased the number of pores with smaller size (0.105-0.160 mm) and so that Young's modulus has increased. Nevertheless, this is supposing that the pores with nanometric size follow the same trend that those analysed by X-ray CT scan (i.e., pores above 40 μm).

4.3 Fracture behaviour

The fracture properties of each mix are presented in Table 5. The tensile strength, f_t, has been determined as one parameter of the bilinear tension softening diagrams (Fig. 9) by the

application of an inverse method based on the non-linear hinge model [63,53], as was described in the previous section. The rest of the parameters of the bilinear softening diagrams are shown in Table 6 for each mix (PC, SFC and LFC). The initial fracture energy, G_f, was determined as the area below the first linear branch of the bilinear softening diagrams (grey zone in Fig. 4) and the total area under the bilinear diagram corresponds with the fracture energy, G_F.

With regards to the tensile strength (Table 4), f_t, slightly decreased with the addition of PP fibres following the trend of the compressive strength results qualitatively. The tensile strength in the concrete reinforced with short PP fibres (SFC) dropped 1.5%, whereas the concrete reinforced with long fibres (LFC) 4.6% compared with the control concrete (i.e., PC). As mentioned, the addition of PP fibres conducted to a concentration of air bubbles around fibres which induced to a large number of pores with higher diameter and volume (Fig. 5 and Table 3) by the pore merging. That increase of pore sizes derives into a reduction of the tensile strength [59].

Table 5 : Average fracture properties and standard deviation.

Mix	f_t (MPa)	G_F (N/m)	G_f (N/m)	l_{ch} (mm)
PC	6.5 (0.2)	83.7 (7.5)	81.2 (7.1)	77.1 (4.5)
SFC	6.4 (0.4)	100.4 (2.0)	96.0 (2.3)	100.3 (3.6)
LFC	6.2 (0.2)	120.9 (9.8)	117.4 (9.4)	135.9 (9.2)

The fracture of concrete is a consequence of the development of the fracture process zone (FPZ) in the material. This process involves a micro-cracking, coalescence, crack branching and frictional interlocking in the weak interfacial transition zone (ITZ) [64]. In this case, the interfacial transition zone would be referred to aggregates and cement paste in the plain concrete (PC) and, additionally, between the fibre and cement paste in the PP fibre reinforced mixes (SFC and LFC). In the FPZ are developed the cohesive normal stresses from a value equal to the tensile strength, at the tip of the crack, until zero at the end of FPZ, in accordance with the widely adopted fictious crack model of Hillerborg [55]. Those cohesive stresses are commonly represented by bilinear softening diagrams, stress-crack opening displacement (Fig. 9).

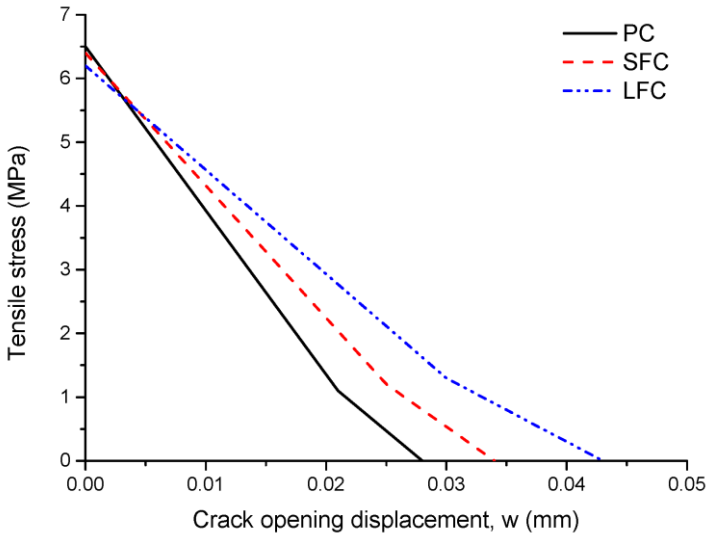

Fig. 9 : Bilinear tension softening diagrams of each mix.

The first linear branch of the bilinear softening diagram is primarily related to the micro-cracking, whereas the second linear branch with the frictional aggregate interlock [39].

The fracture energy results strongly depend on the dosage of the concrete, as postulated by numerous studies [43,44,54,65]. It is worth mentioning that the high content of cement of mixes generates greater shrinkage and provides low fracture energy values in the reference mix (PC). As observed in Table 5, the total fracture energy (G_F) increased with the addition of PP fibres, 17% for SFC and 31% for LFC. It is worth noting as the value of fracture energy corresponded mainly to the initial fracture energy (G_f), with an average percentage of 96.5% G_F. This data together with the values of the slope of the first linear branch, a_1, in Table 6, demonstrate as the microcracking and coalescence are the main processes involve in the fracture mechanisms of these concretes (PC, SFC and LFC).

Table 6 : Parameters of the bilinear tension softening diagrams of each mix.

Mix	a_1 (mm^{-1})	a_2 (mm^{-1})	b_2 (MPa)	w_1 (mm)	w_2 (mm)
PC	40.0	22.4	1.1	0.025	0.028
SFC	37.3	21.0	1.2	0.030	0.034
LFC	29.3	16.8	1.3	0.038	0.043

The slope of the first linear branch risen in those cases of PP fibre reinforced mixes (SFC and LFC) and consequently, the initial fracture energy increased because the presence of PP fibres reduced the number of pores with lower diameter (Fig. 6) and additionally, changed the shape of pores to more spherical. The compression of a porous material mainly leads to compression stresses at the edge of pore and tensile stresses at the pole [66] which derived in the cracking of material when the compressive or tensile maximum stress is achieved. When pores are closer to spherical shapes, the stress concentration (in compression or tension) are lower, as stated by David et al. [66]. With the addition of PP fibres, the pore shape is more spherical (Fig. **7**), especially in the longer PP fibres (LFC), and as a consequence the fracture energy in the cracking process is higher according to the results of Table 5. On the other hand, the

concentration of pores around PP fibres, induced by the presence of them, weakened the adherence between the fibre and cement paste and the frictional interlocking was reduced, as observed from the values of the slope of the second linear branch, a_2, in Table 6. The characteristic length provides information about the ductility of concrete when the specimen size is the same for all tests performed. From the results of Table 5, the ductility (analysed through the characteristic length) of the concretes reinforced with PP fibres significantly risen a 29% for short fibres (i.e., SFC) and a 75% for long fibres (i.e., LFC). This was due to the high number of pores in the matrix (Table 3) which leads to a more ductile material [67]. The increase was significantly higher for long fibre reinforced mix (LFC) because the density of smaller pores is significantly higher, as observed in Table 3. Additionally, the fibres have a bridge effect on the crack front that reduce any microcracking and enhance the ductile behaviour. The bridge effect is more remarkable for longer fibres.

5. Conclusions

The influence of the presence of PP fibres in the microstructure of self-compacting concretes and its consequences in their mechanical and fracture behaviour is a complex analysis that has been thoroughly studied in this work. Three PP fibre-reinforced self-compacting concretes were manufactured. The following conclusions can be drawn from the experimental results:

- The presence of polypropylene fibres in the matrix of concrete reduced the number of smaller pores (i.e., those between 0.10 and 0.20 mm) due to the air bubbles concentration inferred around fibres.

- The concentration of air bubbles around fibres conducted to an increment of the number of pores in the range of pore size 0.25-0.60 mm deriving into a higher amount of larger pores in PP fibre-reinforced mixes (SFC and LFC).

- The mix reinforced with short PP fibres (SFC) presented significantly less amount of pores below 0.1 mm^3 in comparison with that with longer PP fibres (LFC). The higher fibre-matrix interface led to a more significant pore concentration around fibres than in that case of short fibre concrete (SFC). Nevertheless, it was not observed a significant alteration of the microstructure relative to those pore volumes higher than 0.1 mm^3 between SFC and LFC mixes.

- The joining of air bubbles generated beneath fibres leads to a higher sphericity and shape coefficient in PP fibre-reinforced mixes (SFC and LFC). This fact was more remarkable if the PP fibres were shorter (SFC) since the matrix-fibre interface is smaller.

- In the compressive strength, it was observed as the addition of PP fibres conducted to a slight decrease of 3.5% for SFC and 6% for LFC. This decrease was due to the inclusion of a material less resistant (polypropylene fibres) and, additionally, to the increase of the pore size due to the concentration of air bubbles around fibres.

- With regards to the tensile strength, the tensile strength in the concrete reinforced with short PP fibres (SFC) dropped 1.5%, whereas the concrete reinforced with long fibres (LFC) 4.6% compared with respect to the control concrete (PC) due to the increase of pore sizes derives into a reduction of the tensile strength.

- The total fracture energy (G_F) increased with the addition of PP fibres, 17% for SFC and 31% for LFC. It is worth noting as the value of fracture energy corresponded mainly to the initial fracture energy (G_f), with an average percentage of 96.5% G_F. This data together demonstrates as the microcracking and coalescence are the main processes involve in the fracture mechanisms of these concretes (PC, SFC and LFC).

- The initial fracture energy increased on PP fibre-reinforced mixes due to the bridge effect of PP fibres and because the presence of fibres reduced the number of pores with lower diameter. Additionally, changed the shape of pores to more spherical in which the stress concentration is lesser.

- The concentration of pores around PP fibres conducted to the adherence between the fibre and cement paste was additionally weakened and the frictional interlocking was reduced.
- The ductility (determined indirectly by the characteristic length) of the concretes reinforced with PP fibres significantly risen a 29% for short fibres (SFC) and a 75% for long fibres (LFC). This was due to the high number of pores in the matrix, which leads to a more ductile material and the crack bridging of fibres. The increase was significantly higher for long fibre reinforced mix (LFC) because the density of smaller pores is significantly higher and the more efficient adherence of longer fibres.

Acknowledgements

The authors would like to acknowledge the financial support provided to this study by the Spanish Ministry of Economy and Competitiveness (*Ministerio de Economía y Competitividad*) under projects BIA2016-75431-R and the *VI Plan Propio de Investigación* of the University of Seville.

References

[1] Zarnaghi VN, Fouroghi-Asl A, Nourani V, Ma H. On the pore structures of lightweight self-compacting concrete containing silica fume. Construction and Building Materials 2018;193:557–64. doi:10.1016/j.conbuildmat.2018.09.080.

[2] Silva YF, Lange DA, Delvasto S. Effect of incorporation of masonry residue on the properties of self-compacting concretes. Construction and Building Materials 2019;196:277–83. doi:10.1016/j.conbuildmat.2018.11.132.

[3] Silva YF, Robayo RA, Mattey PE, Delvasto S. Properties of self-compacting concrete on fresh and hardened with residue of masonry and recycled concrete. Construction and Building Materials 2016;124:639–44. doi:10.1016/j.conbuildmat.2016.07.057.

[4] Deeb R, Ghanbari A, Karihaloo BL. Development of self-compacting high and ultra high performance concretes with and without steel fibres. Cement and Concrete Composites 2012;34:185–90. doi:10.1016/j.cemconcomp.2011.11.001.

[5] Leemann A, Münch B, Gasser P, Holzer L. Influence of compaction on the interfacial transition zone and the permeability of concrete. Cement and Concrete Research 2006;36:1425–33. doi:10.1016/j.cemconres.2006.02.010.

[6] Leemann A, Loser R, Münch B. Influence of cement type on ITZ porosity and chloride resistance of self-compacting concrete. Cement and Concrete Composites 2010;32:116–20. doi:10.1016/j.cemconcomp.2009.11.007.

[7] Cifuentes H, Leiva C, Medina F, Fernández-Pereira C. Effects of fibers and rice husk ash on properties of heated high-strength concrete. Magazine of Concrete Research 2012;64:457–70. doi:10.1680/macr.11.00087.

[8] Huang H, Gao X, Wang H, Ye H. Influence of rice husk ash on strength and permeability of ultra-high performance concrete. Construction and Building Materials 2017;149:621–8. doi:10.1016/j.conbuildmat.2017.05.155.

[9] Liu J, Yu Q, Zuo Z, Yang F, Duan W, Qin Q. Blast furnace slag obtained from dry granulation method as a component in slag cement. Construction and Building Materials 2017;131:381–7. doi:10.1016/j.conbuildmat.2016.11.040.

[10] Majhi RK, Nayak AN, Mukharjee BB. Development of sustainable concrete using recycled coarse aggregate and ground granulated blast furnace slag. Construction and Building Materials 2018;159:417–30. doi:10.1016/j.conbuildmat.2017.10.118.

[11] Altoubat S, Junaid TM, Leblouba M, Badran D. Effectiveness of fly ash on the restrained shrinkage cracking resistance of self-compacting concrete. Cement and Concrete Composites 2017;79:9–20. doi:10.1016/j.cemconcomp.2017.01.010.

[12] Ozbakkaloglu T, Gu L, Fallah Pour A. Normal- and high-strength concretes incorporating air-cooled blast furnace slag coarse aggregates: Effect of slag size and content on the behavior. Construction and Building Materials 2016;126:138–46. doi:10.1016/j.conbuildmat.2016.09.015.

[13] Santos S, da Silva PR, de Brito J. Self-compacting concrete with recycled aggregates – A literature review. Journal of Building Engineering 2019;22:349–71. doi:10.1016/j.jobe.2019.01.001.

[14] Saccani A, Manzi S, Lancellotti I, Lipparini L. Composites obtained by recycling carbon fibre / epoxy composite wastes in building materials. Construction and Building Materials 2019;204:296–302. doi:10.1016/j.conbuildmat.2019.01.216.

[15] Su Z, Guo L, Zhang Z, Duan P. Influence of different fibers on properties of thermal insulation composites based on geopolymer blended with glazed hollow bead. Construction and Building Materials 2019;203:525–40. doi:10.1016/j.conbuildmat.2019.01.121.

[16] Missemer L, Ouedraogo E, Malecot Y, Clergue C, Rogat D. Fire spalling of ultra-high performance concrete : From a global analysis to microstructure investigations. Cement and Concrete Research 2019;115:207–19. doi:10.1016/j.cemconres.2018.10.005.

[17] Al Qadi ANS, Al-Zaidyeen SM. Effect of fibre content and specimen shape on residual strength of polypropylene fibre self-compacting concrete exposed to elevated temperatures. Journal of King Saud University - Engineering Sciences 2014;26:33–9. doi:10.1016/j.jksues.2012.12.002.

[18] Aarthi K, Arunachalam K. Durability studies on fibre reinforced self compacting concrete with sustainable wastes. Journal of Cleaner Production 2018;174:247–55. doi:10.1016/j.jclepro.2017.10.270.

[19] Hesami S, Hikouei IS, Amir S, Emadi A. Mechanical behavior of self-compacting concrete pavements incorporating recycled tire rubber crumb and reinforced with polypropylene fi ber. Journal of Cleaner Production 2016;133:228–34. doi:10.1016/j.jclepro.2016.04.079.

[20] Ríos JD, Cifuentes H, Leiva C, García C, Alba MD. Behavior of High-Strength Polypropylene Fiber-Reinforced Self-Compacting Concrete Exposed to High Temperatures. Journal of Materials and Civil Engineering, ASCE 2018;30:04018271. doi:10.1061/(ASCE)MT.1943-5533.0002491.

[21] Hwang JP, Kim M, Ann KY. Porosity generation arising from steel fibre in concrete. Construction and Building Materials 2015;94:433–6. doi:10.1016/j.conbuildmat.2015.07.044.

[22] Li D, Li Z, Lv C, Zhang G, Yin Y. A predictive model of the effective tensile and compressive strengths of concrete considering porosity and pore size. Construction and Building Materials 2018;170:520–6. doi:10.1016/j.conbuildmat.2018.03.028.

[23] Kumar R, Bhattacharjee B. Porosity , pore size distribution and in situ strength of concrete 2003;33:155–64.

[24] Ponikiewski T, Katzer J, Bugdol M, Rudzki M. Determination of 3D porosity in steel fibre reinforced SCC beams using X-ray computed tomography. Construction and Building Materials 2014;68:333–40. doi:10.1016/j.conbuildmat.2014.06.064.

[25] Vicente MA, González DC, Mínguez J, Tarifa MA, Ruiz G, Hindi R. Influence of the pore morphology of high strength concrete on its fatigue life. International Journal of Fatigue 2018;112:106–16. doi:10.1016/j.ijfatigue.2018.03.006.

[26] Mastali M, Dalvand A, Sattarifard AR, Abdollahnejad Z, Nematollahi B, Sanjayan JG. A comparison of the effects of pozzolanic binders on the hardened-state properties of high-strength cementitious composites reinforced with waste tire fibers. Composites Part B 2019;162:134–53. doi:10.1016/j.compositesb.2018.10.100.

[27] Khanzadeh Moradllo M, Sudbrink B, Hu Q, Aboustait M, Tabb B, Ley MT, et al. Using micro X-ray fluorescence to image chloride profiles in concrete. Cement and Concrete Research 2017;92:128–41. doi:10.1016/j.cemconres.2016.11.014.

[28] Qsymah A, Sharma R, Yang Z, Margetts L, Mummery P. Micro X-ray computed tomography image-based two-scale homogenisation of ultra high performance fibre

reinforced concrete. Construction and Building Materials 2017;130:230–40. doi:10.1016/j.conbuildmat.2016.09.020.

[29] Suuronen JP, Kallonen A, Eik M, Puttonen J, Serimaa R, Herrmann H. Analysis of short fibres orientation in steel fibre-reinforced concrete (SFRC) by X-ray tomography. Journal of Materials Science 2013;48:1358–67. doi:10.1007/s10853-012-6882-4.

[30] Wang R, Gao X, Zhang J, Han G. Spatial distribution of steel fibers and air bubbles in UHPC cylinder determined by X-ray CT method. Construction and Building Materials 2018;160:39–47. doi:10.1016/j.conbuildmat.2017.11.030.

[31] Ríos JD, Cifuentes H, Leiva C, Seitl S. Analysis of the mechanical and fracture behavior of heated ultra-high-performance fiber-reinforced concrete by X-ray computed tomography. Cement and Concrete Research 2019;119:77–88. doi:10.1016/j.cemconres.2019.02.015.

[32] Ríos JD, Leiva C, Ariza MP, Seitl S, Cifuentes H. Analysis of the tensile fracture properties of ultra-high-strength fiber-reinforced concrete with different types of steel fibers by X-ray tomography. Materials & Design 2019:107582. doi:10.1016/j.matdes.2019.107582.

[33] Pujadas P, Blanco A, Cavalaro S, De la Fuente A, Aguado A. Fibre distribution in macro-plastic fibre reinforced concrete slab-panels. Construction and Building Materials 2014;64:496–503. doi:10.1016/j.conbuildmat.2014.04.067.

[34] Kaufmann J, Frech K, Schuetz P, Münch B. Rebound and orientation of fibers in wet sprayed concrete applications. Construction and Building Materials 2013;49:15–22. doi:10.1016/j.conbuildmat.2013.07.051.

[35] Yermak N, Pliya P, Beaucour A, Simon A, Noumowé A. Influence of steel and/or polypropylene fibres on the behaviour of concrete at high temperature: Spalling, transfer and mechanical properties. Construction and Building Materials 2017;132:240–50. doi:10.1016/j.conbuildmat.2016.11.120.

[36] Fiol F, Thomas C, Muñoz C, Ortega-López V, Manso JM. The influence of recycled aggregates from precast elements on the mechanical properties of structural self-

compacting concrete. Construction and Building Materials 2018;182:309–23. doi:10.1016/j.conbuildmat.2018.06.132.

[37] Ahmad S, Umar A. Rheological and mechanical properties of self-compacting concrete with glass and polyvinyl alcohol fibres. Journal of Building Engineering 2018;17:65–74. doi:10.1016/j.jobe.2018.02.002.

[38] Rehman S, Iqbal S, Ali A. Combined influence of glass powder and granular steel slag on fresh and mechanical properties of self-compacting concrete. Construction and Building Materials 2018;178:153–60. doi:10.1016/j.conbuildmat.2018.05.148.

[39] Alyhya WS, Abo Dhaheer MS, Al-Rubaye MM, Karihaloo BL. Influence of mix composition and strength on the fracture properties of self-compacting concrete. Construction and Building Materials 2016;110:312–22. doi:10.1016/j.conbuildmat.2016.02.037.

[40] Alberti MG, Enfedaque A, Gálvez JC. On the mechanical properties and fracture behavior of polyolefin fiber-reinforced self-compacting concrete. Construction and Building Materials 2014;55:274–88. doi:10.1016/j.conbuildmat.2014.01.024.

[41] Rozière E, Granger S, Turcry P, Loukili A. Influence of paste volume on shrinkage cracking and fracture properties of self-compacting concrete. Cement and Concrete Composites 2007;29:626–36. doi:10.1016/j.cemconcomp.2007.03.010.

[42] Sucharda O, Pajak M, Ponikiewski T, Konecny P. Identification of mechanical and fracture properties of self-compacting concrete beams with different types of steel fibres using inverse analysis. Construction and Building Materials 2017;138:263–75. doi:10.1016/j.conbuildmat.2017.01.077.

[43] Karihaloo BL, Ghanbari A. Mix proportioning of self-compacting high- and ultra-high-performance concretes with and without steel fibres. Magazine of Concrete Research 2012;64:1089–100. doi:10.1680/macr.11.00190.

[44] Deeb R, Karihaloo BL. Mix proportioning of self-compacting normal and high-strength concretes. Magazine of Concrete Research 2013;65:546–56. doi:10.1680/macr.12.00164.

[45] EFNARC. The European Guidelines for Self-Compacting Concrete. The European Guidelines for Self Compacting Concrete 2005:63.

[46] EN-12390-3: 2009. Testing hardened concrete Part 3: Compressive strength of test specimens, AENOR,. Brussels, European Committee for Standarization (CEN): 2009.

[47] EN-12390-13: 2014. Testing hardenes concrete Part 13: Determination of secant modulus of elasticity in compression, AENOR, 2014.

[48] RILEM TC89-FMT 1991. Determination of fracture parameters (KICs and CTODc) of plain concrete using three-point bend tests. Materials and Structures n.d.;23:457–60.

[49] Guinea GV, Planas J, Elices M. Measurement of the fracture energy using three-point bend tests: Part 1- Influence of experimental procedures. Materials and Structures 1992;25:212–8. doi:10.1007/BF02473065.

[50] Planas J, Elices M, Guinea G V. Measurement of the fracture energy using three-point bend tests: Part 2-Influence of bulk energy dissipation. Materials and Structures 1992;25:305–12. doi:10.1007/BF02472671.

[51] Elices M, Guinea GV, Planas J. Measurement of the fracture energy using three-point bend tests: Part 3- Influence of cutting the P-δ tail. Materials and Structures 1992;25:327–34. doi:10.1007/BF02472591.

[52] Abdalla, HM; Karihaloo BL. A method for constructing the bilinear tension softening diagram of concrete corresponding to its true fracture energy. Magazine of Concrete Research n.d.;56. doi:doi.org/10.1680/macr.2004.56.10.597.

[53] Ramachandra Murthy A, Karihaloo BL, Iyer NR, Raghu Prasad BK. Bilinear tension softening diagrams of concrete mixes corresponding to their size-independent specific fracture energy. Construction and Building Materials 2013;47:1160–6. doi:10.1016/j.conbuildmat.2013.06.004.

[54] Cifuentes H, Ríos JD, Gómez EJ. Effect of mix design on the size-independent fracture energy of normal- and high-strength self-compacting concrete. Materiales de Construcción 2018;68:1–11. doi:https://doi.org/10.3989/mc.2018.00717.

[55] Hillerborg, A; Modéer, M;Peterson PE. Analysis of crack formation and crack growth by means of fracture mechanics and finite elements. Cement and Concrete Research 1976:773–82.

[56] Bazant, Z;Planas J. Fracture and size effect in concrete and other quasi brittle materials. Unites States of America, CRC Press 1998.

[57] Al-Azzawi BS, Karihaloo BL. Flexural fatigue behavior of a self-compacting ultrahigh performance fiber-reinforced concrete. Journal of Materials in Civil Engineering 2017;29:04017210. doi:10.1061/(ASCE)MT.1943-5533.0002051.

[58] Zhang B, Bicanic N. Fracture energy of high-performance concrete at high temperatures up to 450°C: the effects of heating temperatures and testing conditions (hot and cold). Magazine of Concrete Research 2006;58:277–88. doi:10.1680/macr.2006.58.5.277.

[59] Chen X, Wu S, Zhou J. Influence of porosity on compressive and tensile strength of cement mortar. Construction and Building Materials 2013;40:869–74. doi:10.1109/SCORED.2003.1459654.

[60] Gencel O, Ozel C, Brostow W, Martínez-Barrera G. Mechanical properties of self-compacting concrete reinforced with polypropylene fibres. Materials Research Innovations 2011;15:216–25. doi:10.1179/143307511X13018917925900.

[61] Cifuentes H, García F, Maeso O, Medina F. Influence of the properties of polypropylene fibres on the fracture behaviour of low-, normal- and high-strength FRC. Construction and Building Materials 2013;45:130–7. doi:10.1016/j.conbuildmat.2013.03.098.

[62] Yoo DY, Shin HO, Yang JM, Yoon YS. Material and bond properties of ultra high performance fiber reinforced concrete with micro steel fibers. Composites Part B: Engineering 2014;58:122–33. doi:10.1016/j.compositesb.2013.10.081.

[63] Abdalla HM, Karihaloo BL. A method for constructing the bilinear tension softening diagram of concrete corresponding to its true fracture energy. Magazine of Concrete Research n.d.;56. doi:doi.org/10.1680/macr.2004.56.10.597.

[64] Scrivener KL, Crumbie AK, Laugesen P. The Interfacial Transition Zone (ITZ) Between Cement Paste and Aggregate in Concrete. Interface Science 2004;12:411–21. doi:10.1023/B:INTS.0000.

[65] Alyhya WS, Dhaheer MSA, Karihaloo BL. Influence of mix composition and strength on the fracture properties of self-compacting concrete. CONSTRUCTION & BUILDING MATERIALS 2016;110:312–22. doi:10.1016/j.conbuildmat.2016.02.037.

[66] Davis T, Healy D, Bubeck A, Walker R. Stress concentrations around voids in three dimensions: The roots of failure. Journal of Structural Geology 2017;102:193–207. doi:10.1016/j.jsg.2017.07.013.

[67] Lian C, Zhuge Y, Beecham S. The relationship between porosity and strength for porous concrete. Construction and Building Materials 2011;25:4294–8. doi:10.1016/j.conbuildmat.2011.05.005.

Detailed responses to the reviewers' comments

Dear editor and reviewers,

We are grateful to the reviewers for taking the time to review our manuscript and for the con- structive suggestions they made. Their comments have helped us to improve the paper. Changes to the original manuscript are given in blue in the revised version. Detailed response to their comments and the explanation of the corresponding changes are given next.

Reviewer #1:

We want to begin by thanking Reviewer #1 for writing that this experimental study is innovative and interesting. We also appreciate the insightful and constructive suggestions. For consistency, we have renumbered the comments. We have addressed all the points raised by the reviewer, as summarized below.

Comments: The authors conducted an innovative, interesting and important research on the influence of the addition of PP fibres on the fracture properties of high-strength self-compacting concrete. An important relation between the materials microstructure and properties on macro level has been given. The special importance of this paper is the comprehensive porosity analysis of the composite based on X-ray computed tomography which compared to the MIP technic give reliable and representative results. The work is well structured, the results logically explained, and conclusions made correct. It could be accepted with suggested minor revisions given in the attached file.

Reply: We have addressed all the minor points raised by the reviewer.

Reviewer #2:

We want to begin by thanking Reviewer #2 for writing that this paper is interesting. We also appreciate the insightful and constructive suggestions. We addressed all the points raised by the reviewer, as summarized below.

Comments: The paper deals with an interesting subject. It needs amendments. Results are similar to those of ordinary concrete. Good insight and discussion are necessary.

Reply: The authors agree that the fracture energy values may be in the range of some normal strength concretes. However, the range of typical values of fracture energy strongly depends on the dosage of the concrete, as shown by the numerous studies focused on this subject [1–4]. The range of possible fracture energy values for NSC and HSC is partially overlapped depending on mix compositions [4,5]. In this study, the fact that the mix proportion has a high content of cement generates greater shrinkage and makes the values of the PC mix (reference concrete) are in the lower fracture energy values of HSC. However, the property to delimit that a concrete is of normal or high strength is the compression. In this paper has been considered high-strength concrete those with a compression value higher than 55 MPa, according to the American Concrete Institute, committee ACI 363 "High-Strength Concrete (ACI 363R)".

Revision has been made in accordance with the reviewer's comment and the following explanation has been included in the text to avoid misunderstanding: "The fracture energy results strongly depend on the dosage of the concrete, as postulated by numerous studies [43,44,55,65]. It is worth mentioning that the high content of cement of mixes generates greater shrinkage and provides lower fracture energy values in the reference mix (PC)."

Other comments are listed below:

1. Do not use carelessly "different". Make it clear as the numbers and the cases.

Reply: Revision has been made in accordance with the reviewer's comments. The authors have given more detailed information by adding numerical data and specifying each case.

2. Sample preparation should be brief. Too instructive.

Reply: Revision has been made in accordance with the reviewer's comments. Sample preparation section has been reduced.

3. All commercial names are to be deleted.

Reply: Revision has been made in accordance with the reviewer's comments. All commercial names have been deleted.

4. Clear scales are necessary in the pictures.

Reply: Revision has been made in accordance with the reviewer's comments. The scales of Figures 6, 7a, 7b and 8 have been modified to clarify the pictures.

5. Findings in Fig. 9 and Table 6 are well known in fiber-reinforced concrete. So what?

Reply: It is true that there are numerous papers that have studied the fracture behaviour of high-strength self-compacting fibre-reinforced concretes but scarce studies have carried out an analysis of the effect of pore structure in the fracture properties of material. Additionally, in this research, the pore structure is analysed by X-ray CT scan and next, it has been stablished a comparison and connection between the fracture properties and the pore structure of each mix which is not performed in other studies. The fracture process strongly depends on the porosity and pore distribution and X-ray CT technique (unlike other techniques) allows to determine the morphology of pores, analysing greater samples more representative of the structural elements in a 3D scale. This is the main approach and contribution of this paper.

6. PhD. thesis is not suitable for the reference, because it is not openly published.

Reply: Revision has been made in accordance with the reviewer's comments. This reference has been deleted.

References

[1] B.L. Karihaloo, A. Ghanbari, Mix proportioning of self-compacting high- and ultra-high-performance concretes with and without steel fibres, Magazine of Concrete Research. 64 (2012) 1089–1100. doi:10.1680/macr.11.00190.

[2] R. Deeb, B.L. Karihaloo, Mix proportioning of self-compacting normal and high-strength concretes, Magazine of Concrete Research. 65 (2013) 546–556. doi:10.1680/macr.12.00164.

[3] W.S. Alyhya, M.S. Abo Dhaheer, M.M. Al-Rubaye, B.L. Karihaloo, Influence of mix composition and strength on the fracture properties of self-compacting concrete, Construction and Building Materials. 110 (2016) 312–322. doi:10.1016/j.conbuildmat.2016.02.037.

[4] H. Cifuentes, J.D. Ríos, E.J. Gómez, Effect of mix design on the size-independent fracture energy of normal- and high-strength self-compacting concrete, Materiales de Construcción. 68 (2018) 1–11. doi:https://doi.org/10.3989/mc.2018.00717.

[5] fib bulletin. N°42, Constitutive modelling for high strength/high performance concrete, 2008. doi:doi.org/10.35789/fib.BULL.0042.

HIGHLIGHTS

- Influence of PP fibres in the pore structure of HSSCC
- Relationship between the macroscopic and microscopic response of HSSCC.
- Relevance of pore morphology in the mechanical and fracture properties of HSSCC.
- Pore morphology and distribution from X-ray tomography analysis

*Declaration of Interest Statement

Declaration of interests

☒ The authors declare that they have no known competing financial interests or personal relationships that could have appeared to influence the work reported in this paper.

☐The authors declare the following financial interests/personal relationships which may be considered as potential competing interests:

Credit Author Statement of the manuscript:

"Microstructural analyses of the addition of PP fibres on the fracture properties of high-strength self-compacting concrete by X-ray computed tomography"

José D. Ríos: Investigation, Methodology, Validation, Writing – Original and Revision. **Jesús Mínguez:** Investigation, Validation, Visualization, Writing – Original and Revision. **Antonio Martínez-De La Concha:** Formal analysis, Visualization, Writing – Original and Revision. **Miguel Ángel Vicente:** Conceptualization, Resources, Writing – Original and Revision. **Héctor Cifuentes:** Conceptualization, Visualization, Supervision, Funding acquisition, Writing – Original and Revision.

Microstructural analyses of the addition of PP fibres on the fracture properties of high-strength self-compacting concrete by X-ray computed tomography

José D. Ríos[a], Jesús Mínguez[b], Antonio Martínez-De La Concha[a], Miguel Ángel Vicente[b] and Héctor Cifuentes[a*]

[a]ETS de Ingeniería. Universidad de Sevilla. Camino de los descubrimientos, s/n. 41092 Sevilla, Spain

[b]Department of Civil Engineering. Escuela Politécnica Superior. Campus Milanera. Universidad de Burgos. 09006 Burgos, Spain

*Corresponding author: bulte@us.es (Héctor Cifuentes)

Abstract

This paper analyses the influence of the presence of polypropylene fibres in the microstructure of a high-strength self-compacting concrete by X-ray computed tomography and its consequences on the mechanical and fracture properties. The addition of PP fibres alters the pore structure of the concrete matrix, and this affects the macroscopic response (i.e., mechanical and fracture behaviour). A microstructural analysis of an unreinforced concrete, used as reference mix, and two polypropylene fibre-reinforced mixes with two fibre length (6 and 24 mm) were experimentally carried out. Complementary, a comprehensive experimental study of the mechanical and fracture properties of each concrete were performed. Finally, it was established a correlation between the microscopic response (pore morphology and pore distribution) and the macroscopic behaviour of high-strength self-compacting concrete.

Keywords: high-strength concrete, polypropylene, fracture mechanic, X-ray computed tomography, microstructure.

Microstructural analyses of the addition of PP fibres on the fracture properties of high-strength self-compacting concrete by X-ray computed tomography

José D. Ríos[a], Jesús Mínguez[b], Antonio Martínez-De La Concha[a], Miguel Ángel Vicente[b] and Héctor Cifuentes[a*]

[a]ETS de Ingeniería. Universidad de Sevilla, Spain
[b]Department of Civil Engineering. Universidad de Burgos, Spain

*Corresponding author: bulte@us.es (Héctor Cifuentes)

Abstract

This paper analyses the influence of the presence of polypropylene fibres in the microstructure of a high-strength self-compacting concrete by X-ray computed tomography and its consequences on the mechanical and fracture properties. The addition of PP fibres alters the pore structure of the concrete matrix, and this affects the macroscopic response (i.e., mechanical and fracture behaviour). A microstructural analysis of an unreinforced concrete, used as reference mix, and two polypropylene fibre-reinforced mixes with two fibre length (6 and 24 mm) were experimentally carried out. Complementary, a comprehensive experimental study of the mechanical and fracture properties of each concrete were performed. Finally, it was established a correlation between the microscopic response (pore morphology and pore distribution) and the macroscopic behaviour of high-strength self-compacting concrete.

Keywords: high-strength concrete, polypropylene, fracture mechanic, X-ray computed tomography, microstructure.

1. Introduction

Self-compacting concrete (SCC) is regarded as one of the most used construction material worldwide [1,2] mainly due to the favourable properties in fresh (e.g. workability, pumpability, finishability) and hardened state (e.g. strength, density, permeability, durability) [3]. This concrete must be as fluid as possible with a stable mix to avoid segregation of solids. The fluidity is achieved commonly with the addition of super-plasticiser and/or viscosity modifying admixtures, and the stability of mix is obtained primarily through proper selection of powders (i.e., cement and cement replacement) [4]. Additionally, these characteristics conduct to a higher packing density (i.e., a reduction of porosity) which combined with the benefits of fibre addition derive to enhanced mechanical and fracture properties in comparison with vibrated concretes [2,3,5,6].

In self-compacting concrete with high compressive strength is very generalised the use of several industrial waste as cement replacement (e.g. fly ash, steel slag, rice husk) [7–11] and / or aggregate substitute (e.g., air-cooled blast furnace slag, masonry waste) [2,12,13] as

reflected by the high number of studies related to this issue. This behaviour conducts principally to two environmental benefits, the reduction of CO_2 emissions by the cement replacement, and complementary, the reuse of waste from several industries. Likewise, polypropylene fibres are also commonly added into the high-strength concretes [1,2,14–17]. The polypropylene fibres reduce the shrinkage effects [18] and enhance fire resistance [19]. Both the substitution of powder or aggregates as well as the fibre addition in the matrix alter the microstructure of concrete and the pore morphology [1,20,21]. Thus, the characteristics of fibres or constituents added have a significant influence in the microstructure and consequently, in the macroscopic response (i.e., mechanical and fracture properties).

The mechanical behaviour of concrete and especially its fracture behaviour, is strongly dependent on the porosity and pore distribution in the material [1,22–25]. There are three types of pores in cementitious matrix depending on the origin generation and their sizes. Gel pores, with characteristic dimensions between 0.5-10 nm; capillary pores, corresponding to the water-filled space ranging from 5 to 5,000 nm and macropores from entrained and entrapped air above 5,000 nm [20,23]. Gel pores have not a significant influence on the strength of material [23]. Nevertheless, capillary pores and macropores (i.e., those due to entrained or entrapped air) affect the strength and stiffness of concrete. There are a large number of researches which have studied the effect of pore structure on fibre-reinforced SCC (i.e., size, distribution, amount) by mercury intrusion porosimetry (MIP) technique [14–16,26]. However, this technique does not allow to capture data of larger pores (i.e., above 40 μm approximately) and the size of samples analysed is too small as being representative of real structural elements. X-ray computed tomography (CT) technique has being increasingly used on cementitious materials [27–31]. This technique allows to determine the geometry of pores (i.e., shape, size, sphericity, volume, etc.) and additionally, to analyse greater samples more representative of the structural elements in a three-dimensional scale.

The appearance of X-ray CT scanning to analyse the microstructure of cementitious materials is relatively recent. Numerous researches have used X-ray CT scan to determine the orientation and distribution of steel fibres on fibre-reinforced primarily concretes [24,29,31,32] since the significant difference of density between steel and concrete make this the ideal technique for this purpose. Nevertheless, there are scarce studies which have used X-ray CT technique in concrete reinforced with polymeric or plastic fibres because the small size of certain fibres makes more difficult their detection by X-ray CT scan. Pujadas et al. [33] analysed the orientation pattern of macro-plastic fibres by X-ray CT scan in which a predominantly perpendicular orientation to the flow of concrete was observed. The orientation of plastic fibres also was the aim of the study by Kaufmann et al. [34] by X-ray CT scan in a spray concrete. In this case, it was determined that the fibres were principally addressing to the perpendicular direction of spray.

Otherwise, some studies have been focused on the influence of pore structure of self-compacting concretes through MIP technique with different purposes. Mastali et al. [26] studied the effects of pozzolanic binders on the hardened-state properties of concrete. Saccani et al. [14] evaluated the effects in the interphase fibre-matrix of composites reinforced with

carbon fibres. However, the most common focus on interest is the thermal effects in the matrix. Missemer et al. [16] characterised the sensitivity of fibre-reinforced concrete to spalling and proposed a critical quantitative factor to determine a fire-resistant composition. Yermark et al. [35] presented a comprehensive study which correlated the mechanical properties with the thermal damage of concrete. Although there are a significant number of studies that have studied the mechanical [19,36–38] and fracture properties [39–42] of self-compacting concrete, scarce investigations have been focused on the porosity evolution inside concrete and the correlation with the macroscopic response (i.e. mechanical and fracture properties).

This work is focused on the effect that the addition of polypropylene fibres in the microstructure of high-strength self-compacting concrete (HSSCC) and its influence on the mechanical and fracture properties. For this, a plain concrete, used as reference concrete, and two PP fibre-reinforced concretes were experimentally assessed. The microstructural analysis of the matrix was performed by X-ray computed tomography technique. Finally, it was established a correlation among the microstructural results obtained by X-ray computed tomography and the mechanical and fracture behaviour of each concrete. The influence of the presence of PP fibres as well as the pore morphology in the fracture mechanisms have been comprehensively analysed.

This paper is organised as follows: a presentation of the materials manufactured, and a description of the sample preparation are shown in Section 2. A description of the experimental programme is exposed in Section 3. The results and discussion are presented in Section 4, and finally, the conclusions are found in Section 5.

2. Materials

2.1 Raw materials and mix designs

In this research, three concretes composed of the same constituents, except that instead of polypropylene fibres, have been manufactured. The mixes were designed following the method proposed by Karihaloo and Ghanbari [43], and Deeb and Karihaloo [44] for self-compacting ordinary and high-strength concretes. The nomenclature and fibre content of the mixes are presented in **Table 1**. The former mix, used as control concrete, is an unreinforced concrete and it is denoted as PC (plain concrete). The second and third of concretes mixes are reinforced with two types of PP fibres. The properties of PP fibres used are the same, except that of length, as can be seen in **Table 1**. The mix labelled as SFC (short-fibre concrete) contains PP fibres of 6 mm in length and the mix designated as LFC (long-fibre concrete) has fibres of 24 mm in length. The amount of PP fibres added to the mixes was the same in both cases (i.e., SFC and LFC) as well as the properties of PP fibres (i.e., thickness and toughness, see **Table 1**). The PP fibre length is the only difference so that the study is focused on the influence of fibre length in the microstructure of mixes.

Table 1 : Nomenclature of mixes, PP fibre content and properties.

	fibre type	fibre content (kg/m^3)	thickness (µm)	toughness (MPa)
PC[a]	no fibres	0	-	-
SFC[b]	6 mm in length	1.2	33	450
LFC[c]	24 mm in length	1.2	33	450

[a] plain concrete, [b] short-fibre concrete, [c] long-fibre concrete.

The mix proportions of constituents used are shown in **Table 2**. The concrete paste has a low water-to-binder ratio which infers a higher performance in terms of mechanical properties to the control concrete (i.e., PC). The binder is formed by type II Portland cement and densified silica fume of 0.1 µm particle size. Three types of aggregates are used (**Table 2**), one designated as fine silica sand, with a maximum particle size of 1 mm, coarse silica sand with a maximum particle size of 10 mm and a limestone sand with 2 mm of maximum size. The grading distribution of the aggregates are shown in Fig. 1.a. A third-generation polycarboxylate-based superplasticiser is used as water reducer. Slump flow tests of each mix, according to EFNARC recommendations [45], were conducted in order to ensure the flowability of concrete paste without segregation (Fig. 1.b).

Table 2 : Mix compositions of plain concrete (kg/m^3)

w/b[a]	cement[b]	silica fume	fine silica sand	coarse silica sand	limestone sand	water	superplasticiser
0.17	657	99	867	1301	139	131	23

[a] w/b water-to-binder ratio, [b] Portland cement (CEM II B-L 32.5 N).

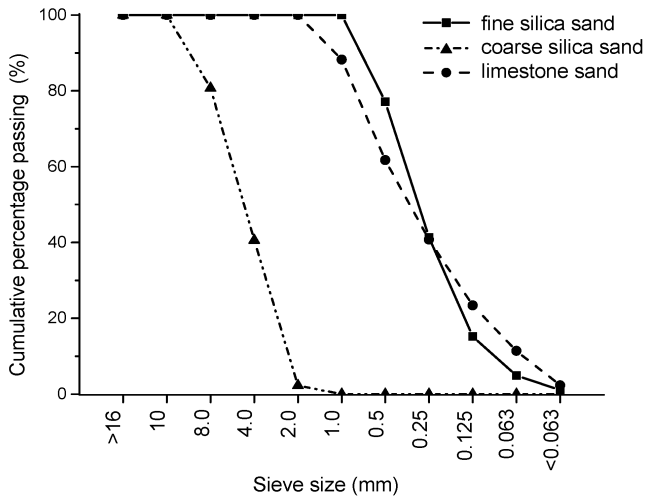

(a)

(b)

Fig. 1: Grading distribution of aggregates (a) and slump flow test of LFC mix (b).

2.2 Sample preparation

The specimen production was always carried out following the same mixing procedure in order to ensure minimising the experimental scattering. A laboratory horizontal rotary mixer was used for the manufacturing of mixes. First the constituent with coarser particle size (i.e., coarse silica sand) is poured in the mixer during the mixing process, next the finer particle size constituent (i.e., silica fume) is added and so, alternatively and subsequently, with the rest of dry constituents (i.e., limestone aggregate, cement and fine silica sand respectively). All dry constituents are mixing for 5 min to ensure a uniform mix. Then, a mix of the water and superplasticiser is poured, and it is mixed for 10 min. When a self-compacting paste is reached the PP fibres are added (for SFC and LFC mixes) and then mixed for 5 min more until fibres are homogeneously dispersed in the concrete paste (Fig. 1.b). The specimens were demoulded after casting for one day and stored in water at ambient temperature for 27 days more. After curing time, the specimens were dried at ambient temperature for 1 day.

3 Methods

In this section, the X-ray CT scanning and the mechanical and fracture tests performed are described.

3.1. Microstructural analysis by X-ray CT scan

X-ray computed tomography scans were carried out for each mix in order to obtain the effect of two PP fibre length (i.e., length of 6 mm and 24 mm) on the microstructure of self-compacting high-strength concrete. For this, three samples of each mix (PC, SFC and LFC) have been scanned in order to minimise the scattering derived from the intrinsic heterogeneity of the material. The samples scanned by X-ray CT had a dimension of 25×25×100 mm^3 and were sawn from beam specimens of 100×100×440 mm^3 casted. A schematic view of the specimen and the samples extracted is shown in **Fig. 2**. The samples were sawn from the core of the specimen and the same part for each mix to avoid border effects that might alter the microstructure of matrix, and consequently, the X-ray CT results obtained.

The CT scan used was a GE Phoenix v|tome|x device (General Electric, Boston, MA, USA), belonging to the 'Centro Nacional de Investigación sobre la Evolución Humana (CENIEH)', in Burgos, Spain. It is equipped with a tube of 300 kV/500 W. This facility emits a cone ray, which is received by an array of detectors. Thereby, the scanning process is fast, and highly accurate scans are produced of equal resolution in the X, Y, and Z axes.

The CT scan provides 16 bits pictures of 2,048×2,048 pixels. From each specimen we obtained 5,000 section images with a pixel size of 0.02. Also, the separation of each section slice was 0.02 mm.

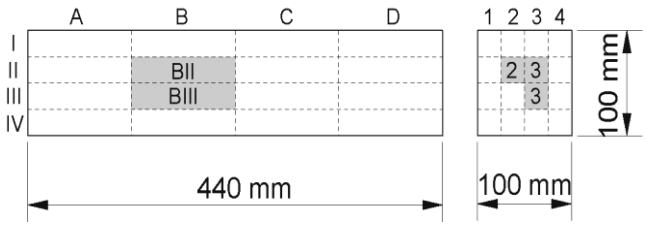

Fig. 2: Scheme of X-ray samples sawn.

Multiple 2D radiographs of each sample scanned were taken by X-ray CT with a scanning resolution of 1,024×1,024 pixels. The commercial software AVIZO was used for the 3D reconstruction of samples scanned (Fig. 3.a, b and c) and the subsequent microstructural analysis of pore properties (i.e., pore equivalent diameter, sphericity, pore surface and shape coefficient). The beam hardening and ring effects [28] were reduced by post-process tools from the analysis software. The equivalent diameter corresponds to the diameter of a sphere with the same volume of the pore, and it is defined as:

$$d_{eq} = \sqrt[3]{6V_{pore} / \pi} \quad (1)$$

Whereby V_{pore} is the volume of a pore. The sphericity of a pore represents how closely the shape of a pore approaches that of a perfect sphere and is defines as:

$$\varphi = \frac{\pi^{1/3}\left(6V_{pore}\right)^{2/3}}{A_{pore}} \quad (2)$$

whereby V_{pore} is the volume of a pore and A_{pore} is the surface area of a pore. The sphericity of a sphere is one and any pore which is not a sphere will have values below 1. The pore surface corresponds to the total area that the surface of the pore occupies. The shape coefficient is a dimensionless property that describes the shape of a pore independently of its size and it is defined as:

$$\alpha = \frac{A_{pore}^{\ 3}}{36\pi V_{pore}^{\ 2}} \quad (3)$$

For more detailed information about the X-ray CT analysis procedure, see the previous work by Rios et al. [32].

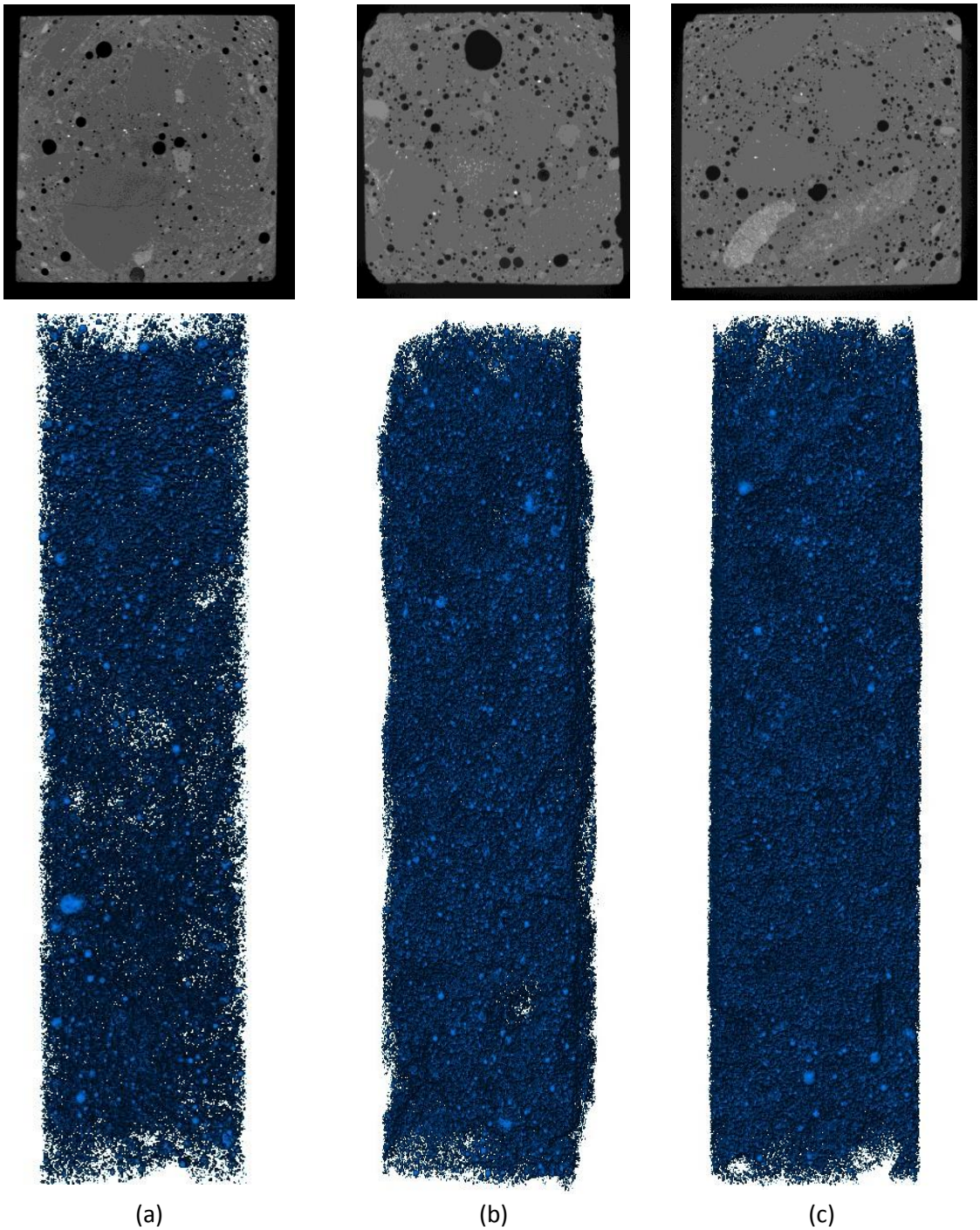

(a) (b) (c)

Fig. 3 : 3D reconstruction of each samples scanned by X-ray CT (a) PC, (b) SFC and (c) LFC mix.

3.2. Mechanical property tests

The compressive strength, f_c, of each mix (i.e. PC, SFC and LFC) were measured from the testing of cubic specimens of 100 mm of side. Four cube specimens of each mix were tested in accordance with the European standard EN-12390-3:2009 [46]. A servo-hydraulic machine of 3,000 kN as maximum load capacity was used with a loading rate of 0.5 MPa/s. The Young's modulus, E_c, was determined by cylindrical specimens of 100 mm diameter and 200 mm height according to the EN-12390-13:2014 [47]. Four specimens were tested of each mix (i.e., PC, SFC

and LFC) and the same servo-hydraulic machine used for compression was used. The procedure consists on the application of a gradual loading until a third of its failure load, and simultaneously, the relative strain is measured by two linear variable displacement transducer (LVDT) sensors of 25 mm in length.

3.3. Fracture property tests

Four specimens of each mix (i.e., PC, SFC and LFC) were conducts on three-point bending tests on notched prismatic specimens of 100×100×440 mm^3 (*B*×*D*×*L*) and notch depth, *a*, of 50 mm to determine the size-independent fracture energy, G_F, by the RILEM method [48] and considering the recommendations suggested by Guinea et al. [49–51]. The tests were conducted on a servo-hydraulic dynamic machine of ± 200 kN and the deflection at the midspan of the specimen was measured by an LVDT sensor of 25 mm. The sensor was mounted on a rigid frame fixed to the specimen. Additionally, the bilinear tension softening diagrams (Fig. 4) of each mix (i.e., PC, SFC and LFC) were determined by the use of an inverse analysis method based on the non-linear hinge model [52,53]. The method is based on the fictitious crack model which is commonly used for the analysis of cracked concrete structures using finite element models [53]. The bilinear softening diagram is defined by the tensile strength, f_t, the slope of the first linear branch, a_1, the slope of the second linear branch, a_2, and its intersection with the ordinate axis, b_1.

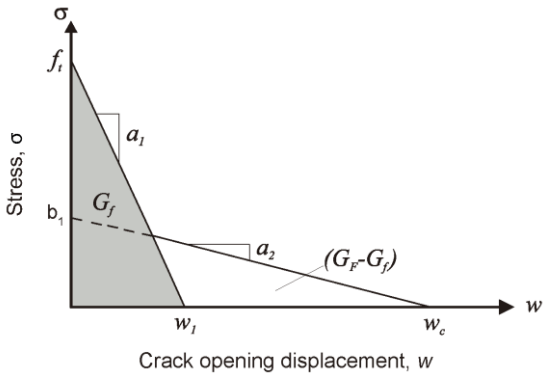

Fig. 4: Bilinear tension softening diagram.

The bilinear tension softening diagram is a proper way to analyse the effect of microstructure in concretes since it provides information about the micro-cracking and frictional dissipation processes responsible for the post-peak behaviour in concrete [39]. The initial fracture energy, G_f, corresponding to the area under the first linear branch (grey zone in Fig. 4), is depending on the microcracking process, while the second linear branch is a result of the frictional dissipation (e.g. aggregate interlock or fibre adherence) [39,54]. That information can be correlated with the X-ray CT results and establish a connection between microstructure and fracture behaviour.

On the other hand, it has been calculated the characteristic length, l_{ch}, which is a fracture parameter that provides information about the intrinsic brittleness of the cohesive material [55]. It is directly related to the fracture process zone (FPZ) due to a greater characteristic

length, higher FPZ [56]. Since all specimens tested had the same dimensions, there was no size effect, and an analysis of the ductility of mixes could be carried out. The characteristic length was calculated as according to Eq. 6:

$$l_{ch} = \frac{G_F E_c}{f_t^2} \quad (6)$$

4 Results and discussion

In this section are shown the results obtained by the X-ray computed tomography so that the effect of PP fibres on the microstructure of mixes can be related with the mechanical and fracture behaviour.

4.1 Microstructural analysis

The use of X-ray CT scan to analyse the microstructure of concrete allows the determination of a wide information about the pore properties (e.g., pore size, surface area, sphericity, etc.) with an accuracy of 40 μm in a large volume of material (Fig. 4). This leads to obtain more reliable results of microstructure in comparison with other techniques in which the volume of material analysed is remarkably more reduced (e.g., mercury intrusion porosimetry). Four prismatic samples of 100×25×25 mm^3 were analysed by X-ray CT scan for each mix (PC, SFC and LFC) and an average value of each pore property measured was obtained in order to reduce the scattering of results due to intrinsic heterogeneity of microstructure [57]. In this work, pores with less than 0.03 voxels (i.e., below 0.1 mm length approximately) are discarded because they are too small to be identified with enough definition [25].

From the X-ray CT results, the diagrams of the equivalent diameter of pores (abscissa axis) and its frequency (ordinate axis) are shown in Fig. 5 and 6 for each mix (PC, SFC and LFC). Pore equivalent diameter in a range between 0.10 and 0.60 mm is presented in Fig. 5 and a detailed diagram of the range of smaller pores, between 0.100-0.225 mm, is shown in Fig. 6 to be more clearly observed. The frequency of pores higher than 0.60 mm is significantly low so that it has not been shown in Fig. 5 since it does not provide relevant information.

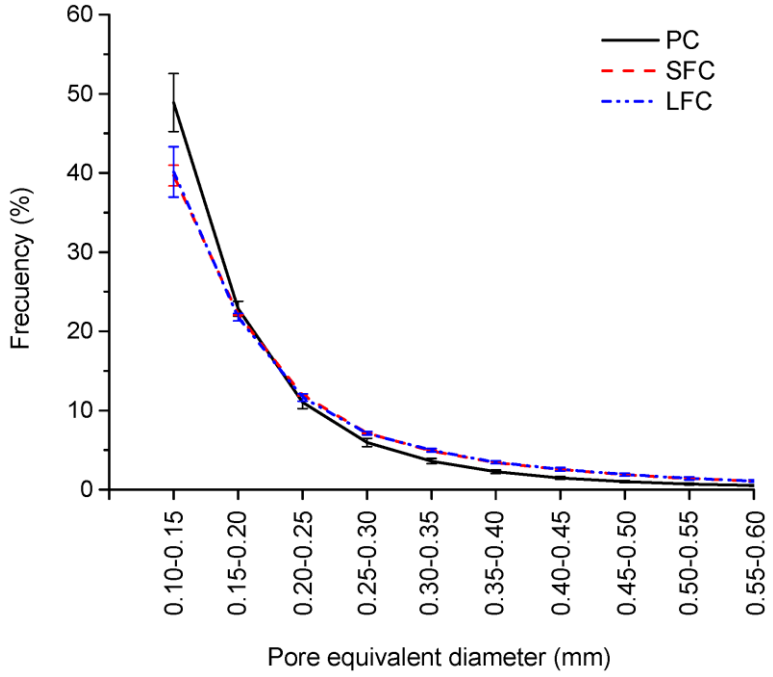

Fig. 5: Distribution of pore equivalent diameter of mixes.

From the results of Fig. 5, it is observed as the control concrete (i.e., PC) has a microstructure with a predominant concentration of pores in the smaller equivalent diameter, the 50% of pores are in the range of 0.10-0.15 mm (see Fig. 5). The presence of polypropylene fibres (SFC and LFC mixes) reduced the number of smaller pores (i.e., between 0.10 and 0.20 mm). The equivalent diameter between 0.10-0.15 mm was reduced 10% in comparison with the control concrete (i.e., PC), due to the air bubbles concentration inferred around fibres according to the results obtained by other authors [21,32]. This conducts to an increment of the equivalent diameter, due to pore fusion by concentrated air bubbles, in the range of pore size 0.25-0.60 mm (see Fig. 5). It is not observed significant differences in the microstructure of those mixes with PP fibres (SFC and LFC), as observed in the overlapping of their curves.

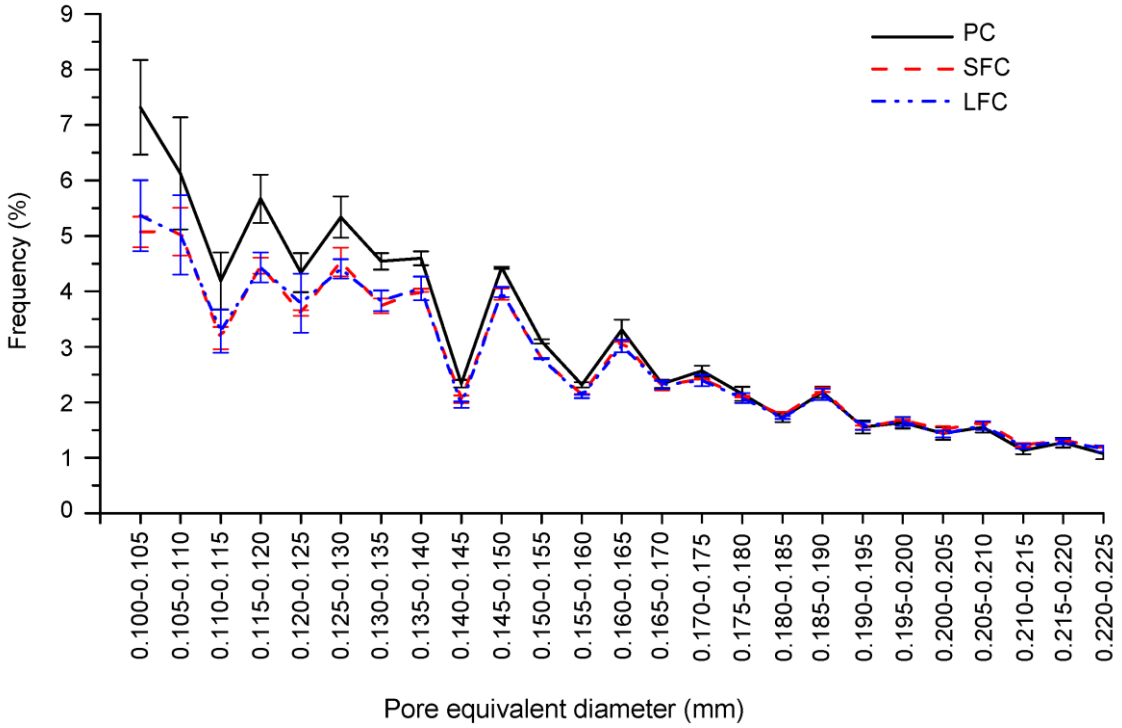

Fig. 6: Pore equivalent diameter of mixes with diameter below 0.225 mm.

Fig. 6 presents the information about those pores with equivalent diameter below 0.22 mm since it has been observed that the presence of PP fibres affects significantly to these pores and it was not able to observe changes, clearly, in the scale of Fig. 5. As observed, the control concrete (PC) has pores with smaller equivalent diameter than those reinforced with PP fibres (SFC and LFC) in the range between 0.100-0.175 mm. That difference is more remarkable for diameter size below 0.140 mm (see Fig. 6). This confirms that the addition of PP fibres increases the pore size by air bubbles concentration around fibres [21,32], as was seen in Fig. 5. The variation on the amount of pores with equivalent diameter between 0.175-0.225 mm is almost non-existent.

Table 3 : Pore density of mixes.

Mix	Pore density (pores/cm^3)				Total porosity (%)
	> 1 mm^3	1-0.5 mm^3	0.5-0.1 mm^3	<0.1 mm^3	
PC	2.0 ± 0.5	2.3 ± 0.6	27 ± 8	4423 ± 1309	2.6 ± 0.7
SFC	2.5 ± 0.5	4.2 ± 0.8	57 ± 5	6923 ± 608	5.4 ± 0.3
LFC	2.2 ± 0.6	3.1 ± 1.3	55 ± 24	10555 ± 444	7.0 ± 0.4

Table 3 presents pore density (in pores/cm^3) for pore volumes higher than 0.1 mm^3, in which the number of pores is low and, as a consequence, those pores could not be shown in Fig. 5 and 6. With regards to the control concrete (PC), it is the mix with a lower number of pores for any volume higher than 0.1 mm^3. This confirms that the plain concrete has a microstructure with pores of a smaller size than those with fibres [32]. In the PP fibre reinforced concretes (SFC and LFC), the mix with shorter PP fibres (SFC) presented significantly less amount of pores

below 0.1 mm^3 in comparison with that with longer PP fibres (LFC). The higher fibre-matrix interface led to a more significant pore concentration around fibres than in that case of short fibre concrete (SFC). Nevertheless, it was not observed a significant alteration of microstructure relative to those pore volumes higher than 0.1 mm^3 between SFC and LFC mixes. It can be confirmed that the PP fibre length studied (6 and 24 mm) has a significant influence only in those pores with volumes below 0.1 mm^3.

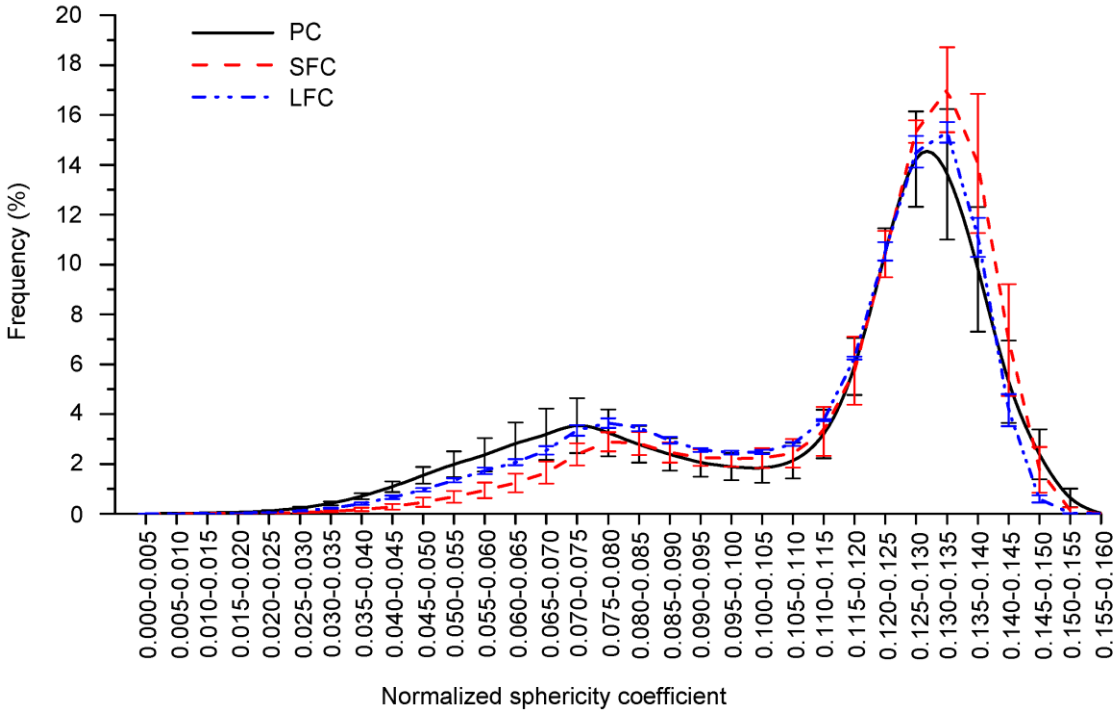

(a)

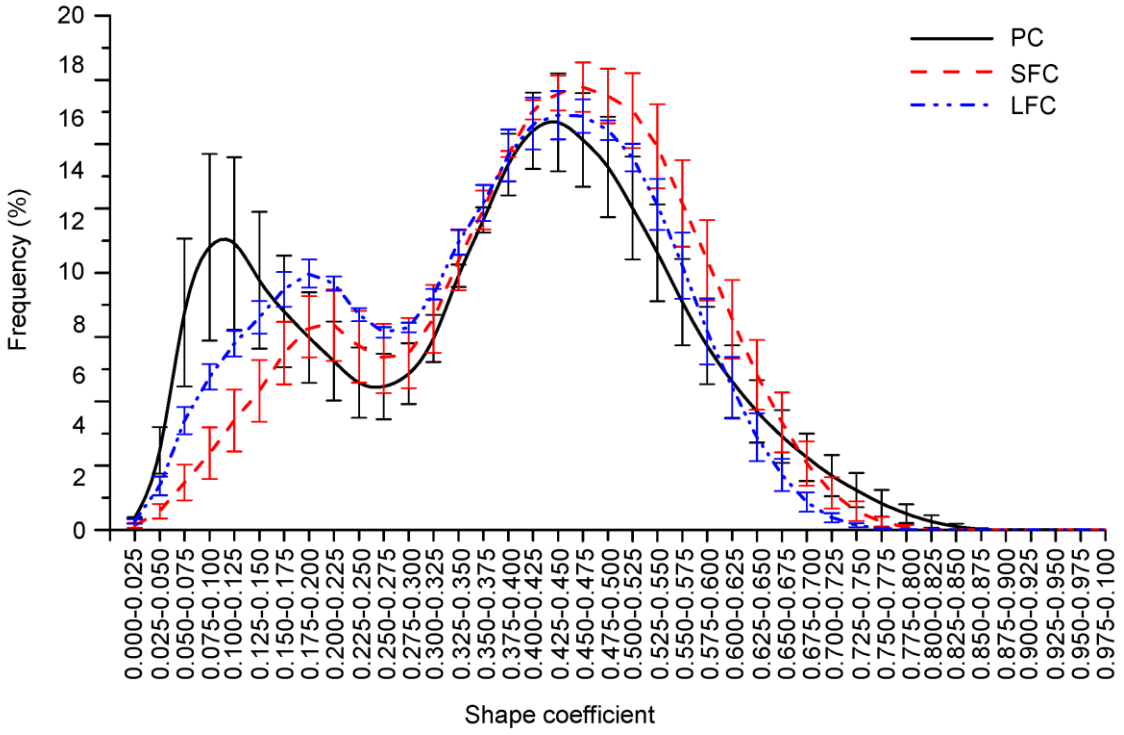

(b)

Fig. 7 : Sphericity (a) and shape coefficient (b) of pores for each mix.

Fig. 7 shows the values of the sphericity and shape coefficient of pores for each mix (PC, SFC and LFC). Both properties, the sphericity and shape coefficient, are an indication of the pore shape, which is related to each other as follows: $\varphi = \frac{1}{\alpha^{1/3}}$. For this reason, the discussion of the results is made jointly. The range of sphericity values (Fig. 7.a) varies between 0.000-0.160, which shows that the shape of pores is not very spherical for any mix, control (PC) or PP fibre-reinforced concrete (SFC and LFC). With regards to PP fibre reinforced mixes, the join of air bubbles generated beneath fibres leads to a higher sphericity (Fig. 7.a) and shape coefficient (Fig. 7.b). This was observed in the horizontal displacement (i.e., into higher spherical pore) of the peak points of Fig. 7.a and b for SFC and LFC mixes in comparison with PC mix. Additionally, there is a decrease of the shape coefficient in the range 0.150-0.175 and a complementary increase in the range 0.475-0.500 that confirms as pores are more spherical. This fact is more remarkable if the PP fibres are shorter (i.e., SFC) than longer (i.e. LFC) due to the decrease in the range of 0.150-0.175 of shape coefficient is significantly higher than LFC. By contrast, the increase in the range 0.475-0.500 of shape coefficient is higher than LFC mix.

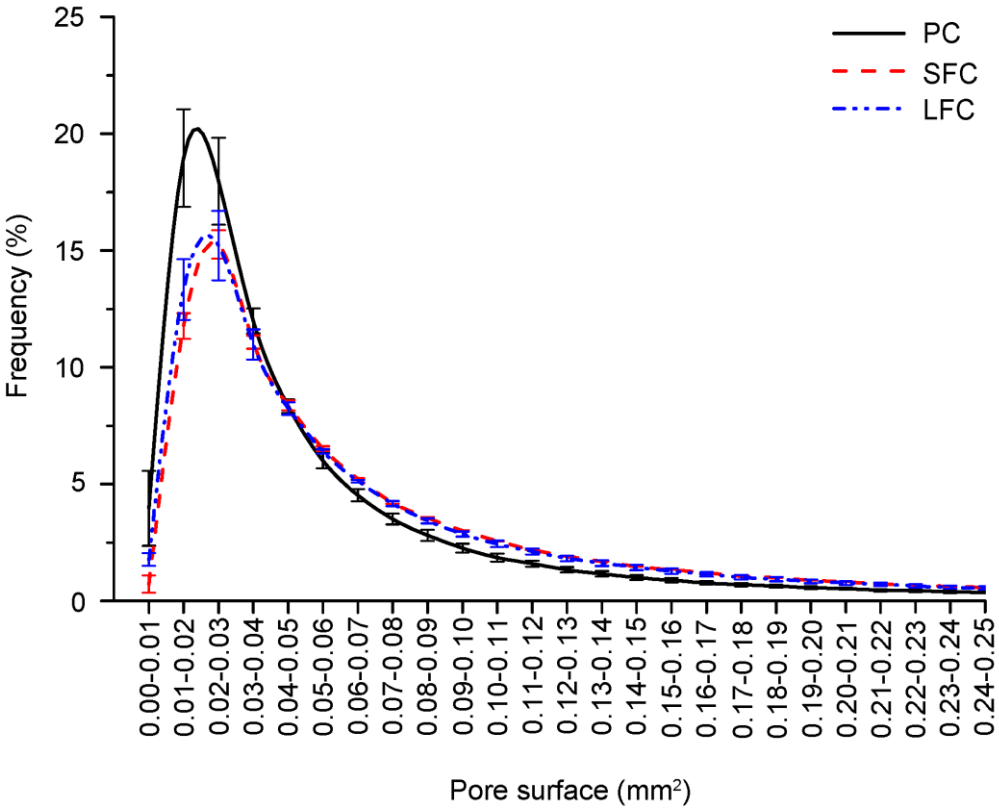

Fig. 8 : Pore surface of each mix

The pore surface results for each mix (PC, SFC and LFC) are shown in Fig. 8. From the control concrete (i.e., PC), there is a higher number of pores with surface area lower than those in PP fibre reinforced mixes (SFC and LFC). As shown, the 20% of pores are in the range of pore

surface between 0.01-0.04 whereas the PP fibre reinforced mixes (SFC and LFC) have a 16% in the same interval (see **Error! Reference source not found.**). The mesh of air bubbles generated around PP fibres leads to pores with higher volumes (as shown Table 3) and more spherical (Fig. 7**Error! Reference source not found.**.a and b) so that the surface area of pores must be higher, as shown in Fig. 8.

4.2 Mechanical properties

The average value of the compressive strength and Young's modulus, corresponding to the tests described in the previous section, and their standard deviation are shown in Table 4 for each SCC mix.

Table 4 : Average mechanical properties and standard deviation.

Mix	f_c (MPa)	E_c (GPa)
PC	80.0 (7.4)	38.9 (3.4)
SFC	77.2 (3.9)	40.9 (1.1)
LFC	75.2 (4.8)	43.2 (1.7)

From the results of compressive strength, it is observed as the addition of PP fibres conducted to a slight decrease of 3.5% for SFC and 6% for LFC. Other authors observed this fact in similar conditions [20,58]. This decrease was due to the inclusion of a material less resistant (i.e., polypropylene fibres) to the compressive stresses during the test and the alteration of microstructure by the presence of PP fibres, as presented in total porosity results (Table 3). The incidence of microstructure on the compressive strength of cement-based materials has been significantly studied by several researchers [22,23,25,59]. Many relationships that are establishing a connection between the compressive strength and pore structure of material have been obtained [22,59]. Thus, the decrease of compressive strength by the addition of PP fibres is due to the inclusion of a material less resistance (i.e., polypropylene fibres) and, additionally, to the increase of the total porosity, the pore size and amount of pores lower than 0.1 mm^3, due to the concentration of air bubbles around fibres reflected by the higher values of equivalent diameter (Fig. 5 and 6) and density (Table 3) respectively.

Regarding Young's modulus, the PP fibre reinforced mixes (SFC and LFC) slightly increased, 5.1% on SFC and 11% on LFC, following the results obtained by other authors [20,60,61]. As known, this property is primarily influenced by a higher number of pores with a size of nanometres, rather than a lower amount of pores with larger sizes [62]. From the results shown in Fig. 6, it is observed that the addition of PP fibres decreased the number of pores with smaller size (0.105-0.160 mm) and so that Young's modulus has increased. Nevertheless, this is supposing that the pores with nanometric size follow the same trend that those analysed by X-ray CT scan (i.e., pores above 40 μm).

4.3 Fracture behaviour

The fracture properties of each mix are presented in **Table 5**. The tensile strength, f_t, has been determined as one parameter of the bilinear tension softening diagrams (**Fig. 9**) by the

application of an inverse method based on the non-linear hinge model [63,53], as was described in the previous section. The rest of the parameters of the bilinear softening diagrams are shown in **Table 6** for each mix (PC, SFC and LFC). The initial fracture energy, G_f, was determined as the area below the first linear branch of the bilinear softening diagrams (grey zone in Fig. 4) and the total area under the bilinear diagram corresponds with the fracture energy, G_F.

With regards to the tensile strength (Table 4), f_t, slightly decreased with the addition of PP fibres following the trend of the compressive strength results qualitatively. The tensile strength in the concrete reinforced with short PP fibres (SFC) dropped 1.5%, whereas the concrete reinforced with long fibres (LFC) 4.6% compared with the control concrete (i.e., PC). As mentioned, the addition of PP fibres conducted to a concentration of air bubbles around fibres which induced to a large number of pores with higher diameter and volume (Fig. 5 and Table 3) by the pore merging. That increase of pore sizes derives into a reduction of the tensile strength [59].

Table 5 : Average fracture properties and standard deviation.

Mix	f_t (MPa)	G_F (N/m)	G_f (N/m)	l_{ch} (mm)
PC	6.5 (0.2)	83.7 (7.5)	81.2 (7.1)	77.1 (4.5)
SFC	6.4 (0.4)	100.4 (2.0)	96.0 (2.3)	100.3 (3.6)
LFC	6.2 (0.2)	120.9 (9.8)	117.4 (9.4)	135.9 (9.2)

The fracture of concrete is a consequence of the development of the fracture process zone (FPZ) in the material. This process involves a micro-cracking, coalescence, crack branching and frictional interlocking in the weak interfacial transition zone (ITZ) [64]. In this case, the interfacial transition zone would be referred to aggregates and cement paste in the plain concrete (PC) and, additionally, between the fibre and cement paste in the PP fibre reinforced mixes (SFC and LFC). In the FPZ are developed the cohesive normal stresses from a value equal to the tensile strength, at the tip of the crack, until zero at the end of FPZ, in accordance with the widely adopted fictious crack model of Hillerborg [55]. Those cohesive stresses are commonly represented by bilinear softening diagrams, stress-crack opening displacement (**Fig. 9**).

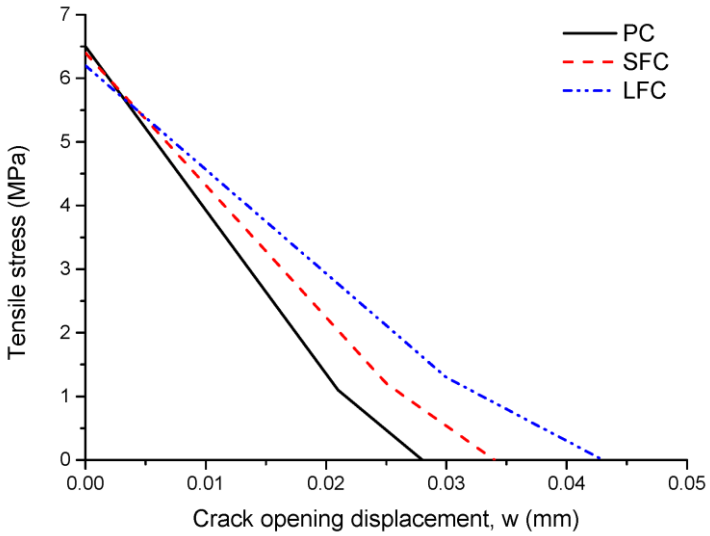

Fig. 9 : Bilinear tension softening diagrams of each mix.

The first linear branch of the bilinear softening diagram is primarily related to the micro-cracking, whereas the second linear branch with the frictional aggregate interlock [39].

The fracture energy results strongly depend on the dosage of the concrete, as postulated by numerous studies [43,44,54,65]. It is worth mentioning that the high content of cement of mixes generates greater shrinkage and provides low fracture energy values in the reference mix (PC). As observed in Table 5, the total fracture energy (G_F) increased with the addition of PP fibres, 17% for SFC and 31% for LFC. It is worth noting as the value of fracture energy corresponded mainly to the initial fracture energy (G_f), with an average percentage of 96.5% G_F. This data together with the values of the slope of the first linear branch, a_1, in **Table 6**, demonstrate as the microcracking and coalescence are the main processes involve in the fracture mechanisms of these concretes (PC, SFC and LFC).

Table 6 : Parameters of the bilinear tension softening diagrams of each mix.

Mix	a_1 (mm^{-1})	a_2 (mm^{-1})	b_2 (MPa)	w_1 (mm)	w_2 (mm)
PC	40.0	22.4	1.1	0.025	0.028
SFC	37.3	21.0	1.2	0.030	0.034
LFC	29.3	16.8	1.3	0.038	0.043

The slope of the first linear branch risen in those cases of PP fibre reinforced mixes (SFC and LFC) and consequently, the initial fracture energy increased because the presence of PP fibres reduced the number of pores with lower diameter (Fig. 6) and additionally, changed the shape of pores to more spherical. The compression of a porous material mainly leads to compression stresses at the edge of pore and tensile stresses at the pole [66] which derived in the cracking of material when the compressive or tensile maximum stress is achieved. When pores are closer to spherical shapes, the stress concentration (in compression or tension) are lower, as stated by David et al. [66]. With the addition of PP fibres, the pore shape is more spherical (Fig. **7**), especially in the longer PP fibres (LFC), and as a consequence the fracture energy in the cracking process is higher according to the results of Table 5. On the other hand, the

concentration of pores around PP fibres, induced by the presence of them, weakened the adherence between the fibre and cement paste and the frictional interlocking was reduced, as observed from the values of the slope of the second linear branch, a_2, in Table 6. The characteristic length provides information about the ductility of concrete when the specimen size is the same for all tests performed. From the results of Table 5, the ductility (analysed through the characteristic length) of the concretes reinforced with PP fibres significantly risen a 29% for short fibres (i.e., SFC) and a 75% for long fibres (i.e., LFC). This was due to the high number of pores in the matrix (Table 3) which leads to a more ductile material [67]. The increase was significantly higher for long fibre reinforced mix (LFC) because the density of smaller pores is significantly higher, as observed in Table 3. Additionally, the fibres have a bridge effect on the crack front that reduce any microcracking and enhance the ductile behaviour. The bridge effect is more remarkable for longer fibres.

5. Conclusions

The influence of the presence of PP fibres in the microstructure of self-compacting concretes and its consequences in their mechanical and fracture behaviour is a complex analysis that has been thoroughly studied in this work. Three PP fibre-reinforced self-compacting concretes were manufactured. The following conclusions can be drawn from the experimental results:

- The presence of polypropylene fibres in the matrix of concrete reduced the number of smaller pores (i.e., those between 0.10 and 0.20 mm) due to the air bubbles concentration inferred around fibres.

- The concentration of air bubbles around fibres conducted to an increment of the number of pores in the range of pore size 0.25-0.60 mm deriving into a higher amount of larger pores in PP fibre-reinforced mixes (SFC and LFC).

- The mix reinforced with short PP fibres (SFC) presented significantly less amount of pores below 0.1 mm^3 in comparison with that with longer PP fibres (LFC). The higher fibre-matrix interface led to a more significant pore concentration around fibres than in that case of short fibre concrete (SFC). Nevertheless, it was not observed a significant alteration of the microstructure relative to those pore volumes higher than 0.1 mm^3 between SFC and LFC mixes.

- The joining of air bubbles generated beneath fibres leads to a higher sphericity and shape coefficient in PP fibre-reinforced mixes (SFC and LFC). This fact was more remarkable if the PP fibres were shorter (SFC) since the matrix-fibre interface is smaller.

- In the compressive strength, it was observed as the addition of PP fibres conducted to a slight decrease of 3.5% for SFC and 6% for LFC. This decrease was due to the inclusion of a material less resistant (polypropylene fibres) and, additionally, to the increase of the pore size due to the concentration of air bubbles around fibres.

- With regards to the tensile strength, the tensile strength in the concrete reinforced with short PP fibres (SFC) dropped 1.5%, whereas the concrete reinforced with long fibres (LFC) 4.6% compared with respect to the control concrete (PC) due to the increase of pore sizes derives into a reduction of the tensile strength.

- The total fracture energy (G_F) increased with the addition of PP fibres, 17% for SFC and 31% for LFC. It is worth noting as the value of fracture energy corresponded mainly to the initial fracture energy (G_f), with an average percentage of 96.5% G_F. This data together demonstrates as the microcracking and coalescence are the main processes involve in the fracture mechanisms of these concretes (PC, SFC and LFC).

- The initial fracture energy increased on PP fibre-reinforced mixes due to the bridge effect of PP fibres and because the presence of fibres reduced the number of pores with lower diameter. Additionally, changed the shape of pores to more spherical in which the stress concentration is lesser.

- The concentration of pores around PP fibres conducted to the adherence between the fibre and cement paste was additionally weakened and the frictional interlocking was reduced.
- The ductility (determined indirectly by the characteristic length) of the concretes reinforced with PP fibres significantly risen a 29% for short fibres (SFC) and a 75% for long fibres (LFC). This was due to the high number of pores in the matrix, which leads to a more ductile material and the crack bridging of fibres. The increase was significantly higher for long fibre reinforced mix (LFC) because the density of smaller pores is significantly higher and the more efficient adherence of longer fibres.

Acknowledgements

The authors would like to acknowledge the financial support provided to this study by the Spanish Ministry of Economy and Competitiveness (*Ministerio de Economía y Competitividad*) under projects BIA2016-75431-R and the *VI Plan Propio de Investigación* of the University of Seville.

References

[1] Zarnaghi VN, Fouroghi-Asl A, Nourani V, Ma H. On the pore structures of lightweight self-compacting concrete containing silica fume. Construction and Building Materials 2018;193:557–64. doi:10.1016/j.conbuildmat.2018.09.080.

[2] Silva YF, Lange DA, Delvasto S. Effect of incorporation of masonry residue on the properties of self-compacting concretes. Construction and Building Materials 2019;196:277–83. doi:10.1016/j.conbuildmat.2018.11.132.

[3] Silva YF, Robayo RA, Mattey PE, Delvasto S. Properties of self-compacting concrete on fresh and hardened with residue of masonry and recycled concrete. Construction and Building Materials 2016;124:639–44. doi:10.1016/j.conbuildmat.2016.07.057.

[4] Deeb R, Ghanbari A, Karihaloo BL. Development of self-compacting high and ultra high performance concretes with and without steel fibres. Cement and Concrete Composites 2012;34:185–90. doi:10.1016/j.cemconcomp.2011.11.001.

[5] Leemann A, Münch B, Gasser P, Holzer L. Influence of compaction on the interfacial transition zone and the permeability of concrete. Cement and Concrete Research 2006;36:1425–33. doi:10.1016/j.cemconres.2006.02.010.

[6] Leemann A, Loser R, Münch B. Influence of cement type on ITZ porosity and chloride resistance of self-compacting concrete. Cement and Concrete Composites 2010;32:116–20. doi:10.1016/j.cemconcomp.2009.11.007.

[7] Cifuentes H, Leiva C, Medina F, Fernández-Pereira C. Effects of fibers and rice husk ash on properties of heated high-strength concrete. Magazine of Concrete Research 2012;64:457–70. doi:10.1680/macr.11.00087.

[8] Huang H, Gao X, Wang H, Ye H. Influence of rice husk ash on strength and permeability of ultra-high performance concrete. Construction and Building Materials 2017;149:621–8. doi:10.1016/j.conbuildmat.2017.05.155.

[9] Liu J, Yu Q, Zuo Z, Yang F, Duan W, Qin Q. Blast furnace slag obtained from dry granulation method as a component in slag cement. Construction and Building Materials 2017;131:381–7. doi:10.1016/j.conbuildmat.2016.11.040.

[10] Majhi RK, Nayak AN, Mukharjee BB. Development of sustainable concrete using recycled coarse aggregate and ground granulated blast furnace slag. Construction and Building Materials 2018;159:417–30. doi:10.1016/j.conbuildmat.2017.10.118.

[11] Altoubat S, Junaid TM, Leblouba M, Badran D. Effectiveness of fly ash on the restrained shrinkage cracking resistance of self-compacting concrete. Cement and Concrete Composites 2017;79:9–20. doi:10.1016/j.cemconcomp.2017.01.010.

[12] Ozbakkaloglu T, Gu L, Fallah Pour A. Normal- and high-strength concretes incorporating air-cooled blast furnace slag coarse aggregates: Effect of slag size and content on the behavior. Construction and Building Materials 2016;126:138–46. doi:10.1016/j.conbuildmat.2016.09.015.

[13] Santos S, da Silva PR, de Brito J. Self-compacting concrete with recycled aggregates – A literature review. Journal of Building Engineering 2019;22:349–71. doi:10.1016/j.jobe.2019.01.001.

[14] Saccani A, Manzi S, Lancellotti I, Lipparini L. Composites obtained by recycling carbon fibre / epoxy composite wastes in building materials. Construction and Building Materials 2019;204:296–302. doi:10.1016/j.conbuildmat.2019.01.216.

[15] Su Z, Guo L, Zhang Z, Duan P. Influence of different fibers on properties of thermal insulation composites based on geopolymer blended with glazed hollow bead. Construction and Building Materials 2019;203:525–40. doi:10.1016/j.conbuildmat.2019.01.121.

[16] Missemer L, Ouedraogo E, Malecot Y, Clergue C, Rogat D. Fire spalling of ultra-high performance concrete : From a global analysis to microstructure investigations. Cement and Concrete Research 2019;115:207–19. doi:10.1016/j.cemconres.2018.10.005.

[17] Al Qadi ANS, Al-Zaidyeen SM. Effect of fibre content and specimen shape on residual strength of polypropylene fibre self-compacting concrete exposed to elevated temperatures. Journal of King Saud University - Engineering Sciences 2014;26:33–9. doi:10.1016/j.jksues.2012.12.002.

[18] Aarthi K, Arunachalam K. Durability studies on fibre reinforced self compacting concrete with sustainable wastes. Journal of Cleaner Production 2018;174:247–55. doi:10.1016/j.jclepro.2017.10.270.

[19] Hesami S, Hikouei IS, Amir S, Emadi A. Mechanical behavior of self-compacting concrete pavements incorporating recycled tire rubber crumb and reinforced with polypropylene fi ber. Journal of Cleaner Production 2016;133:228–34. doi:10.1016/j.jclepro.2016.04.079.

[20] Ríos JD, Cifuentes H, Leiva C, García C, Alba MD. Behavior of High-Strength Polypropylene Fiber-Reinforced Self-Compacting Concrete Exposed to High Temperatures. Journal of Materials and Civil Engineering, ASCE 2018;30:04018271. doi:10.1061/(ASCE)MT.1943-5533.0002491.

[21] Hwang JP, Kim M, Ann KY. Porosity generation arising from steel fibre in concrete. Construction and Building Materials 2015;94:433–6. doi:10.1016/j.conbuildmat.2015.07.044.

[22] Li D, Li Z, Lv C, Zhang G, Yin Y. A predictive model of the effective tensile and compressive strengths of concrete considering porosity and pore size. Construction and Building Materials 2018;170:520–6. doi:10.1016/j.conbuildmat.2018.03.028.

[23] Kumar R, Bhattacharjee B. Porosity , pore size distribution and in situ strength of concrete 2003;33:155–64.

[24] Ponikiewski T, Katzer J, Bugdol M, Rudzki M. Determination of 3D porosity in steel fibre reinforced SCC beams using X-ray computed tomography. Construction and Building Materials 2014;68:333–40. doi:10.1016/j.conbuildmat.2014.06.064.

[25] Vicente MA, González DC, Mínguez J, Tarifa MA, Ruiz G, Hindi R. Influence of the pore morphology of high strength concrete on its fatigue life. International Journal of Fatigue 2018;112:106–16. doi:10.1016/j.ijfatigue.2018.03.006.

[26] Mastali M, Dalvand A, Sattarifard AR, Abdollahnejad Z, Nematollahi B, Sanjayan JG. A comparison of the effects of pozzolanic binders on the hardened-state properties of high-strength cementitious composites reinforced with waste tire fibers. Composites Part B 2019;162:134–53. doi:10.1016/j.compositesb.2018.10.100.

[27] Khanzadeh Moradllo M, Sudbrink B, Hu Q, Aboustait M, Tabb B, Ley MT, et al. Using micro X-ray fluorescence to image chloride profiles in concrete. Cement and Concrete Research 2017;92:128–41. doi:10.1016/j.cemconres.2016.11.014.

[28] Qsymah A, Sharma R, Yang Z, Margetts L, Mummery P. Micro X-ray computed tomography image-based two-scale homogenisation of ultra high performance fibre

reinforced concrete. Construction and Building Materials 2017;130:230–40. doi:10.1016/j.conbuildmat.2016.09.020.

[29] Suuronen JP, Kallonen A, Eik M, Puttonen J, Serimaa R, Herrmann H. Analysis of short fibres orientation in steel fibre-reinforced concrete (SFRC) by X-ray tomography. Journal of Materials Science 2013;48:1358–67. doi:10.1007/s10853-012-6882-4.

[30] Wang R, Gao X, Zhang J, Han G. Spatial distribution of steel fibers and air bubbles in UHPC cylinder determined by X-ray CT method. Construction and Building Materials 2018;160:39–47. doi:10.1016/j.conbuildmat.2017.11.030.

[31] Ríos JD, Cifuentes H, Leiva C, Seitl S. Analysis of the mechanical and fracture behavior of heated ultra-high-performance fiber-reinforced concrete by X-ray computed tomography. Cement and Concrete Research 2019;119:77–88. doi:10.1016/j.cemconres.2019.02.015.

[32] Ríos JD, Leiva C, Ariza MP, Seitl S, Cifuentes H. Analysis of the tensile fracture properties of ultra-high-strength fiber-reinforced concrete with different types of steel fibers by X-ray tomography. Materials & Design 2019:107582. doi:10.1016/j.matdes.2019.107582.

[33] Pujadas P, Blanco A, Cavalaro S, De la Fuente A, Aguado A. Fibre distribution in macro-plastic fibre reinforced concrete slab-panels. Construction and Building Materials 2014;64:496–503. doi:10.1016/j.conbuildmat.2014.04.067.

[34] Kaufmann J, Frech K, Schuetz P, Münch B. Rebound and orientation of fibers in wet sprayed concrete applications. Construction and Building Materials 2013;49:15–22. doi:10.1016/j.conbuildmat.2013.07.051.

[35] Yermak N, Pliya P, Beaucour A, Simon A, Noumowé A. Influence of steel and/or polypropylene fibres on the behaviour of concrete at high temperature: Spalling, transfer and mechanical properties. Construction and Building Materials 2017;132:240–50. doi:10.1016/j.conbuildmat.2016.11.120.

[36] Fiol F, Thomas C, Muñoz C, Ortega-López V, Manso JM. The influence of recycled aggregates from precast elements on the mechanical properties of structural self-

compacting concrete. Construction and Building Materials 2018;182:309–23. doi:10.1016/j.conbuildmat.2018.06.132.

[37] Ahmad S, Umar A. Rheological and mechanical properties of self-compacting concrete with glass and polyvinyl alcohol fibres. Journal of Building Engineering 2018;17:65–74. doi:10.1016/j.jobe.2018.02.002.

[38] Rehman S, Iqbal S, Ali A. Combined influence of glass powder and granular steel slag on fresh and mechanical properties of self-compacting concrete. Construction and Building Materials 2018;178:153–60. doi:10.1016/j.conbuildmat.2018.05.148.

[39] Alyhya WS, Abo Dhaheer MS, Al-Rubaye MM, Karihaloo BL. Influence of mix composition and strength on the fracture properties of self-compacting concrete. Construction and Building Materials 2016;110:312–22. doi:10.1016/j.conbuildmat.2016.02.037.

[40] Alberti MG, Enfedaque A, Gálvez JC. On the mechanical properties and fracture behavior of polyolefin fiber-reinforced self-compacting concrete. Construction and Building Materials 2014;55:274–88. doi:10.1016/j.conbuildmat.2014.01.024.

[41] Rozière E, Granger S, Turcry P, Loukili A. Influence of paste volume on shrinkage cracking and fracture properties of self-compacting concrete. Cement and Concrete Composites 2007;29:626–36. doi:10.1016/j.cemconcomp.2007.03.010.

[42] Sucharda O, Pajak M, Ponikiewski T, Konecny P. Identification of mechanical and fracture properties of self-compacting concrete beams with different types of steel fibres using inverse analysis. Construction and Building Materials 2017;138:263–75. doi:10.1016/j.conbuildmat.2017.01.077.

[43] Karihaloo BL, Ghanbari A. Mix proportioning of self-compacting high- and ultra-high-performance concretes with and without steel fibres. Magazine of Concrete Research 2012;64:1089–100. doi:10.1680/macr.11.00190.

[44] Deeb R, Karihaloo BL. Mix proportioning of self-compacting normal and high-strength concretes. Magazine of Concrete Research 2013;65:546–56. doi:10.1680/macr.12.00164.

[45] EFNARC. The European Guidelines for Self-Compacting Concrete. The European Guidelines for Self Compacting Concrete 2005:63.

[46] EN-12390-3: 2009. Testing hardened concrete Part 3: Compressive strength of test specimens, AENOR,. Brussels, European Committee for Standarization (CEN): 2009.

[47] EN-12390-13: 2014. Testing hardenes concrete Part 13: Determination of secant modulus of elasticity in compression, AENOR, 2014.

[48] RILEM TC89-FMT 1991. Determination of fracture parameters (KICs and CTODc) of plain concrete using three-point bend tests. Materials and Structures n.d.;23:457–60.

[49] Guinea GV, Planas J, Elices M. Measurement of the fracture energy using three-point bend tests: Part 1- Influence of experimental procedures. Materials and Structures 1992;25:212–8. doi:10.1007/BF02473065.

[50] Planas J, Elices M, Guinea G V. Measurement of the fracture energy using three-point bend tests: Part 2-Influence of bulk energy dissipation. Materials and Structures 1992;25:305–12. doi:10.1007/BF02472671.

[51] Elices M, Guinea GV, Planas J. Measurement of the fracture energy using three-point bend tests: Part 3- Influence of cutting the P-δ tail. Materials and Structures 1992;25:327–34. doi:10.1007/BF02472591.

[52] Abdalla, HM; Karihaloo BL. A method for constructing the bilinear tension softening diagram of concrete corresponding to its true fracture energy. Magazine of Concrete Research n.d.;56. doi:doi.org/10.1680/macr.2004.56.10.597.

[53] Ramachandra Murthy A, Karihaloo BL, Iyer NR, Raghu Prasad BK. Bilinear tension softening diagrams of concrete mixes corresponding to their size-independent specific fracture energy. Construction and Building Materials 2013;47:1160–6. doi:10.1016/j.conbuildmat.2013.06.004.

[54] Cifuentes H, Ríos JD, Gómez EJ. Effect of mix design on the size-independent fracture energy of normal- and high-strength self-compacting concrete. Materiales de Construcción 2018;68:1–11. doi:https://doi.org/10.3989/mc.2018.00717.

[55] Hillerborg, A; Modéer, M;Peterson PE. Analysis of crack formation and crack growth by means of fracture mechanics and finite elements. Cement and Concrete Research 1976:773–82.

[56] Bazant, Z;Planas J. Fracture and size effect in concrete and other quasi brittle materials. Unites States of America, CRC Press 1998.

[57] Al-Azzawi BS, Karihaloo BL. Flexural fatigue behavior of a self-compacting ultrahigh performance fiber-reinforced concrete. Journal of Materials in Civil Engineering 2017;29:04017210. doi:10.1061/(ASCE)MT.1943-5533.0002051.

[58] Zhang B, Bicanic N. Fracture energy of high-performance concrete at high temperatures up to 450°C: the effects of heating temperatures and testing conditions (hot and cold). Magazine of Concrete Research 2006;58:277–88. doi:10.1680/macr.2006.58.5.277.

[59] Chen X, Wu S, Zhou J. Influence of porosity on compressive and tensile strength of cement mortar. Construction and Building Materials 2013;40:869–74. doi:10.1109/SCORED.2003.1459654.

[60] Gencel O, Ozel C, Brostow W, Martínez-Barrera G. Mechanical properties of self-compacting concrete reinforced with polypropylene fibres. Materials Research Innovations 2011;15:216–25. doi:10.1179/143307511X13018917925900.

[61] Cifuentes H, García F, Maeso O, Medina F. Influence of the properties of polypropylene fibres on the fracture behaviour of low-, normal- and high-strength FRC. Construction and Building Materials 2013;45:130–7. doi:10.1016/j.conbuildmat.2013.03.098.

[62] Yoo DY, Shin HO, Yang JM, Yoon YS. Material and bond properties of ultra high performance fiber reinforced concrete with micro steel fibers. Composites Part B: Engineering 2014;58:122–33. doi:10.1016/j.compositesb.2013.10.081.

[63] Abdalla HM, Karihaloo BL. A method for constructing the bilinear tension softening diagram of concrete corresponding to its true fracture energy. Magazine of Concrete Research n.d.;56. doi:doi.org/10.1680/macr.2004.56.10.597.

[64] Scrivener KL, Crumbie AK, Laugesen P. The Interfacial Transition Zone (ITZ) Between Cement Paste and Aggregate in Concrete. Interface Science 2004;12:411–21. doi:10.1023/B:INTS.0000.

[65] Alyhya WS, Dhaheer MSA, Karihaloo BL. Influence of mix composition and strength on the fracture properties of self-compacting concrete. CONSTRUCTION & BUILDING MATERIALS 2016;110:312–22. doi:10.1016/j.conbuildmat.2016.02.037.

[66] Davis T, Healy D, Bubeck A, Walker R. Stress concentrations around voids in three dimensions: The roots of failure. Journal of Structural Geology 2017;102:193–207. doi:10.1016/j.jsg.2017.07.013.

[67] Lian C, Zhuge Y, Beecham S. The relationship between porosity and strength for porous concrete. Construction and Building Materials 2011;25:4294–8. doi:10.1016/j.conbuildmat.2011.05.005.